X-646-71-199

PROPERTIES OF LOW ENERGY PARTICLE IMPACTS IN THE POLAR DOMAIN IN THE DAWN AND DAYSIDE HOURS

R. A. HOFFMAN

JUNE 1971

GSFC
GODDARD SPACE FLIGHT CENTER
GREENBELT, MARYLAND

PROPERTIES OF LOW ENERGY PARTICLE IMPACTS IN THE POLAR DOMAIN IN THE DAWN AND DAYSIDE HOURS

By

R. A. Hoffman
Goddard Space Flight Center
Greenbelt, Maryland

June 1971

Paper presented at the Magnetosphere-Ionosphere Interactions Advanced Study Institute, Espedalen, Norway, April 15-22, 1971.

PROPERTIES OF LOW ENERGY PARTICLE IMPACTS IN THE POLAR DOMAIN IN THE DAWN AND DAYSIDE HOURS

R. A. Hoffman
Goddard Space Flight Center
Greenbelt, Maryland

Abstract

In the dawn and dayside hours of the polar domain, two regions of electron precipitation have been identified: a very high latitude - "soft zone", and a lower latitude "hard zone".

The electrons in the soft zone produce a large number of interesting phenomena both above and in the ionosphere, such as the generation of VLF hiss, magnetic effects from the currents they constitute, electron concentration enhancement peaks at 1000 km altitudes, and the dayside auroral oval, with emissions predominantly at 6300Å. Electron precipitation in this zone is continuously present.

On the other hand, fewer phenomena appear associated with the lower latitude hard zone, which exists through the morning hours to noon, and is related to substorm activity. The higher energy precipitating electrons (> 50 keV) produce D-layer events. The lower energy electrons (a few keV) produce the mantle aurora, but because of a likely energy dispersion from local time drift of the electrons originating in the midnight region, the morphology of E-layer absorption events is more difficult to observe.

INTRODUCTION

Two regions of electron precipitation have been identified in the dawn and dayside hours of the polar domain, a very high latitude "soft zone" and a lower latitude "hard zone". The characteristics of the radiation in the two regions, that is, the energy spectrums, structure and morphology, are entirely different as well as the relationship of the radiation to magnetic activity. The electron precipitation in the "soft zone" produces a large number of interesting phenomena both above and in the ionosphere. On the other hand fewer phenomena appear associated with the lower latitude "hard zone".

In this review the particle precipitation regions will first be defined. Their spectral and spatial characteristics will be displayed and their relationship with magnetic activity exhibited. The second part of the review will discuss the effects of the "soft zone" precipitation both above and in the ionosphere, including the generation of VLF hiss, magnetic effects from the currents the precipitation constitutes, electric effects, ionization effects, and production of the dayside auroral oval. The third part of the review will emphasize the relationship of the lower latitude "hard zone" with the morphology of ionospheric absorption events, as well as the production of the mantle aurora.

The data base for this review is data from the OGO-4 Auroral Particles Experiment, although considerable use will be made of data from other satellites and ground stations.

PART 1. DEFINITION OF PARTICLE PRECIPITATION REGIONS

The definition of the particle precipitation regions in the dayside and morning hours of the magnetosphere is based primarily on measurements made of low energy precipitating electrons in the energy range of 100 ev to tens of kilovolts. In the morning hours up until local noon two regions have been identified, the lower latitude hard zone (68^{o} to 75^{o}) and a higher latitude soft zone (75^{o} to 80^{o}). After local noon only the soft zone appears to be present. A polar cavity exists at latitudes above about 80^{o}, where only small fluxes of electrons precipitate.

A. Examples of Measurements in the Regions

The first really clear evidence of the existence of two regions of precipitation at high latitudes was obtained by the Lockheed group from two short-lived satellite flights in 1963 and 1965, (Sharp and Johnson, 1968). In the 1965 flight the detection of the soft zone was made by a differential energy detector measuring electrons at an energy of about 1 kilovolt, whereas the detection of the "hard zone" was made by an integral energy detector measuring electrons having energies greater than about 9 kilovolts (Figure 1). While only a few passes of data were available the data clearly showed the existence of the two zones. On the same satellite a detector measuring protons having energies greater than about 21 kilovolts gave indication of the possibility of two zones of proton precipitation as well. Note in the figure that the centers of the dayside precipitation regions have been plotted, not the extent of the regions of precipitation.

Additional information regarding the existence of two precipitation regions came from the Aurora 1 satellite (Burch, 1968). In Figure 2 a very weak hard zone extending from about 62° to 75° can be seen in the detector measuring electrons in the energy range 6.2 to 25 keV. The soft zone appears in the 46 to 280 ev channel, commencing abruptly at a latitude of 75° and ending at 80°. A small portion of the polar cavity appears at latitudes above 80°.

More extensive measurements of the morning and daytime precipitation regions have been made with the Auroral Particles Experiment on the OGO-4 satellite (Hoffman, 1969). Figure 3 contains data comparing the regions of precipitation in the afternoon and morning hours. This pass of data begins in the afternoon hours at a latitude of 70° where there is no evidence of a low latitude hard zone because of the lack of electrons at 7.3 keV below 78°. The soft zone commences at a latitude of 75° where the 0.7 keV detector counting rate begins to show structure, exists through the noontime hours even at a latitude of 84.6° and ends abruptly in the morning hours at 79°. The morning hour lower latitude hard zone is evident in the counting rate from the 7.3 keV detector and commences at a latitude of about 75° and extends down to about 69° at a local time of about 7.5 hours. Another example from the OGO-4 satellite (Figure 4) reveals especially clearly the two regions of precipitation as well as the polar cavity.

More recent measurements of these precipitation regions have been made by a detector having excellent energy resolution aboard the ISIS-1 satellite (Heikkila and Winningham, 1971). Data from a pass in the late morning hours are shown in Figure 5. The top portion of the figure contains

a spectrogram from precipitating electrons, where the density of the trace qualitatively indicates the spectral energy density as a function of particle energy. The hard zone can be identified by the presence of electrons in the energy interval 10^3 to 10^4 ev from an invariant latitude of 66° to about 74°. For this pass the precipitation produced a total energy flux of about 0.1 ergs/cm^2-sec-ster. The soft zone is characterized by precipitating electrons having an energy slightly above 10^2 ev, and extends from 74° to almost 80° invariant latitude. The almost total lack of precipitation with energies above 10^2 ev at latitudes higher than 80° indicates the polar cavity.

B. Spectrums in the Regions

Typical energy spectrums obtained in the soft zone from three different experiments appear in Figure 6. Only the ISIS-1 electron spectrometer measured sufficiently low energy electrons with adequate energy resolution to identify a peak in the spectrum at about 100 ev. Data from the Aurora-1 and OGO-4 experiments indicate an extremely steep energy spectrum at energies above the peak in the spectrum. The particle flux falls off at least as steep as E^{-3} at energies above a couple 100 ev. This figure indicates that data from the lowest energy channels of the latter two experiments, 46 to 280 ev on Aurora-1 and 0.7 keV on OGO-4, do indeed indicate the presence of the soft zone.

The hard zone appears dominantly at energies from 1-10 keV (Figure 7), and often displays a knee in the energy spectrum between 5 to 10 keV. Note that the 0.7 keV detector on OGO-4 measured a flux only about 10 times the flux at 7.3 keV, whereas, in Figure 6 the ratio of these two fluxes was more like a factor of 10^3. It is on the bases of the grossly

different spectrums as well as structures in the two regions that in the remainder of this paper we use the output of the 0.7 keV detector as an indicator of the soft zone and the 7.3 keV detector as the indicator of the hard zone.

C. Spatial Extent of the Regions

The spatial extent and frequency of occurrence of the soft zone have been studied using data from the 0.7 keV detector aboard OGO-4 (Hoffman and Berko, 1971). For this study all data from the 0.7 keV detector collected from July 30, 1967, through February 26, 1968, were analyzed. The criteria used to define this region were rapid fluctuations in the counting rate from the detector with peak electron fluxes of at least 10^8 electrons/cm^2-sec-ster-keV. An attempt was made to eliminate the effects of magnetic activity especially in the midnight region. Data were used during times when K_p was less than or equal to 2. Additional data were eliminated in the mid-night region on the basis that precipitating electrons with fairly hard energy spectrums are usually associated with magnetic activity even though the counting rate profiles may be highly structured (see Fig. 14 from 70^o to 73^o) (Hoffman, 1969). Therefore when the counting rate of the 7.3 keV detector rose rapidly and in coincidence with increases in the 0.7 keV detector counting rate it was assumed that the precipitation was associated with magnetic activity and these data were simply not counted.

The resulting soft zone frequency of occurrence map appears in Figure 8. The most striking feature of this map is the concentration of high probabilities (i.e., $\geq 40\%$) between 5 and 14 hours and from 75^o to $82\frac{1}{2}^o$ invariant latitudes in these hours. On the nightside the probabilities

are generally smaller and tend to appear at lower latitudes than during the daytime hours. The probabilities in the daytime hours are so high that one finds the soft zone to be always present. (See Hoffman and Berko, 1971, for the distribution of samples used to prepare Figure 8.)

To again exemplify that data from the 0.7 keV detector on OGO-4 could define the soft zone, at least during the daytime hours, we have superimposed the location of the soft zone as defined by data from ISIS-1 and Aurora-1 on a simplified version of the frequency of occurrence map (Figure 9). The spectral and spatial considerations presented give us confidence that data from the OGO-4 experiment can indeed be used to determine certain properties of the soft zone radiation.

We next wish to investigate the dependence of the soft zone on magnetic activity and universal time. For these studies we have measured the low latitude and high latitude boundaries of the soft zone as defined by the response of the 0.7 keV detector on OGO-4 when the satellite was within two hours and three hours respectively of local magnetic noon. The latitude of these boundaries as a function of K_p are plotted in the upper two panels of Figure 10 and the average locations of the boundaries for each integral value of K_p in the lower panels for data acquired during the late winter and early summer of 1968. The magnetic parameter K_p appears to order the location of the lower boundary better than the location of the upper boundary. It is surprising that such a magnetic parameter which depends upon the nightside auroral electrojet should produce any ordering in the location of the daytime soft zone. This implies that the location of the soft zone is dependent upon the magnetospheric configuration rather than upon any local magnetic effects. The movement of the soft zone is almost 2^o equatorward for each value of K_p.

We next plot the upper boundary location and the lower boundary location as a function of universal time for those passes when $K_p \leq 1+$. In neither case does there appear to be a U.T. effect greater than about 2^o. In the top portion of Figure 11 we have included data from the Aurora-1 satellite (Maehlum, 1968), which indicated a rather strong U.T. effect. Unfortunately geomagnetic activity during the early portion of the lifetime of Aurora-1 as measured by K_p indicated moderate activity; in fact, at least two of the four data points between 6 and 10 hours U.T. occurred when K_p was 3+ and 4. Taking into account the shift in latitude of the upper boundary of the soft zone with increasing K_p as well as the fairly large scatter of data points at moderate K_p's (see Figure 10), it appears possible that the Aurora-1 data might be explained as a magnetic effect rather than a U.T. variation.

A universal time control of phenomena occurring at high latitudes can be ascribed to the variation in angle which the geomagnetic axis makes with the earth-sun line (β) as a function of U.T., and therefore the solar wind flow direction, (Maehlum, 1969). This variation in tilt could cause geomagnetic field distortions which vary the boundary locations. In the northern hemisphere the geomagnetic axis dips towards the sun near 1800 to 2000 U.T. and away from the sun near 0600 to 0800 U.T. Since the tilt of the geomagnetic axis is even more dependent upon the season of the year, we have plotted all upper boundary locations when $K_p \leq 1+$ as a function of β in Figure 12. The data points with β greater than 100^o were acquired primarily during February, whereas the data points less than 90^o were acquired primarily in late April and May. The winter time data show less scatter of the data points than the summer time data. The least squares fit of a linear relationship to all the data points shows

not more than a combined $2\frac{1}{2}^{o}$ seasonal and U.T. variation in the high latitude boundary of the soft zone.

So far all boundary studies have been performed using low energy electron precipitation data. The ISIS-1 experiment also measured low energy protons which seem to occur concurrent with the electron precipitation although more narrowly confined in latitude (Winningham, 1970). While only a small amount of proton precipitation data are available, the location of this region also seems to depend strongly upon K_p (Figure 13). In the figure we have indicated by each data point the geomagnetic tilt angle β. Note that for the lower boundary, when K_p=1-, the tilt angle varied between 60^{o} and 104^{o} for the three data points, yet the boundary changed by less than 3^{o}. Thus the proton precipitation displays the same relations to magnetic activity and tilt angle as electron precipitation.

While it was previously suggested by Vernov (1966) and Thomas (1966), there is now evidence that the high latitude soft zone is due to direct penetration of the magnetosheath plasma to low altitudes through the dayside magnetospheric cusps (Heikkila and Winningham, 1971; Frank, 1970). The soft zone would then occur necessarily on open field lines and the low latitude boundary would be nearly synonymous with the last closed field line on the dayside. If this is the case, one can explain the lack of U.T. control and the strong dependence on magnetic activity on the location of the dayside soft zone by the following. While the outer reaches of the magnetosphere may be distorted in various ways by a variation in the tilt of the geomagnetic axis, the number of closed field lines on the dayside would remain the same, thus negating any low altitude effect. On the other hand the number of closed field lines and, therefore

the latitude of the last closed field line when measured at low altitudes, would be more strongly dependent upon the magnetospheric configuration, which changes during magnetic activity (Cummings et al, 1968).

We next turn to the location of the hard zone. Because the hard zone extends into the midnight regions, we show in Figure 14 data obtained from a near midnight pass of the OGO-4 satellite in order to define the region at such hours. These data were acquired during a geomagnetic substorm. Large fluxes of 7.3 keV electrons were observed precipitating between latitudes of 60° and 66°, but especially note the small fluctuations in the counting rate from the detector. At higher latitudes from 70° to 73° this detector measured even larger fluxes, but they occurred exactly in coincidence with very large fluxes at 0.7 keV. At these hours we will again define the hard zone as the region of 7.3 keV precipitation with rather small fluctuations in the counting rate from the detector.

On the basis of these criteria the location of the hard zone is shown in Figure 15. Note that it begins in the early evening hours about 1900 M.L.T., continues through midnight at its lowest latitude (64 to 68½ degrees) and ends at local noon in the latitude range of about 70 to 74 degrees. On only very few occasions out of about 200 passes through the afternoon hours has anything even resembling a hard zone been observed. In the figure the spatial definition of the hard zone is based upon all observations, independent of magnetic activity. Note that the upper boundary of the hard region and the lower boundary of the soft zone are nearly coincident. On an individual pass basis these two boundaries may be slightly separated, such as in Figure 3, or at times slightly overlapped, such as in Figure 4.

Previously we presented evidence (Hoffman, 1970) that the electrons precipitating in the hard zone originate on closed field lines in the midnight region at the time of substorms, and subsequently drift around through the morning hours, where they encounter a strong pitch angle scattering mechanism to cause the precipitation. The character of the radiation throughout the entire region is essentially the same (Hoffman and Berko, 1971a). The average energy spectrum everywhere is similar to that shown in Figure 7. As evidence of this we plot in Figure 15 the ratio of 0.7 keV to 7.3 keV flux at three different local times as a function of invariant latitude. There appears to be a slight tendency towards softening of the spectrum to higher latitudes, although this situation is not always observed on a pass to pass basis.

If indeed these electrons do drift in local time on close field lines we must explain the large 5 to 6 degree shift in latitude from midnight to noon in the boundaries of the region. In such a model we must assume that a particle measured as precipitating at a particular local time has spent most of its lifetime with a mirror point near the magnetic equator where the bulk of particles in normal distributions are always found. The magnetospheric distortions can account for only about 1 to 2 degrees shift in latitude in the lower boundary of this region (Fairfield, 1968). The apparent increased distortion could be accounted for by several things. First, in the late morning hours at latitudes just below the indicated lower boundary of the hard zone, the fluxes could be too low for measurement. Since the longitudinal drift time is inversely related to latitude, the population could have been depleted prior to arrival at the late morning hours. Second, the electrons could be driven out towards

the boundary of the magnetosphere by electric fields. There is a slight bit of evidence for cross-L drift because the ratios in Figure 16 indicate a slight softening with increase in latitude. On the other hand it could equally as well indicate an inward drift with a slight energization of the electrons.

PART II. EFFECTS OF SOFT ZONE PRECIPITATION

In the second part of the review we will discuss the effects of the soft zone precipitation as a function of decreasing height; that is, as the electrons proceed from the outer regions of the magnetosphere down into the atmosphere they produce different phenomenon. These effects are divided into five categories, auroral hiss, magnetic effects, both DC and AC, electric effects, ionization effects, and the dayside auroral oval.

A. Auroral Hiss

Auroral hiss is a wide-band noise observed from a few hertz to several hundred khz at high magnetic latitudes. It is generally ascribed to the incoherent Cerenkov radiation process, where emissions are generated from incoming electrons with velocities that exceed or are comparable to the phase velocity of the radiation in the medium (Jørgensen, 1968). If the hiss propagates in the whistler mode it will occur at frequencies below the plasma cutoff, and below the electron cyclotron frequency, but above the local lower hybrid resonance. In his paper, Jørgensen discussed a model for a region in space in which the auroral hiss is believed to be generated. He showed that the total power generated in this region is comparable to the observed power, and concluded that auroral hiss may be generated by incoherent Cerenkov radiation from electrons with energies

of the order of 1 keV. He acknowledged the fact that the inclusion of electrons with energies below 1 keV in his calculations of the noise spectrum would increase his spectral density, but could not perform the calculations because the knowledge of auroral electrons with energies below 1 keV was very poor at that time.

Hartz (1970) studied the broad-band noise emissions observed by Alouette II in the frequency range of the Cerenkov radiation. On the basis of the spatial distribution of this noise he concluded that the emissions arose from the Cerenkov radiation and were related to fluxes of electrons having energies in the range 0.1 to 1 keV. From the general characteristics of the noise band he concluded that the region of generation was localized to the height interval near and not too far above the satellite.

We have compared the electron precipitation measurements from the OGO-4 satellite with the VLF observations from an electric dipole antenna on the same satellite (Laaspere and Hoffman, 1971)(Figure 17). Data in this figure show the general coincidence of the region of 0.7 keV electron precipitation with the region of auroral hiss. The hiss seems to spread slightly beyond the location of the particle precipitation, especially to lower latitudes. Figure 18 contains one of the VLF records for comparison with electron precipitation at energies above a kilovolt. The broad, rather structureless, region of precipitation defines the location of the hard zone. While the hiss begins to appear in this region of harder radiation it is dominantly at higher latitudes. By these two figures we show that the auroral hiss is associated with electrons having energies less than a kilovolt and is not related to the precipitation in the hard zone.

In general it is difficult to find a one-to-one correlation between specific bursts of electrons and a dominant feature in the auroral hiss. This would be expected because of some propagation of hiss across field lines, as well as the fact that the particle measurements refer to the precipitation measured at an extremely small cross section of magnetic lines of force. However, in Figure 19 we do show an exact relationship between the 0.7 keV precipitation and a particular auroral hiss event. In this case a very isolated burst of the 0.7 keV electrons was observed with no appreciable precipitation for some tens of seconds on either side. By far the most prominent feature in the VLF record occurs simultaneously with the burst of electrons. The very dark feature at the end of the VLF record is due to loss of satellite telemetry signal.

These correlations between VLF and particle precipitation events are easiest to find in the morning hours in the soft zone. The general relationship between the auroral hiss and the soft zone is shown in Figure 20. This figure contains VLF data from electric dipole experiments aboard OGO-6 and Alouette II satellites. The dots are the locations of the centers of 200 khz radiation measured from the OGO-6 satellite (Laaspere, 1971), whereas the contours of 200 khz radiation were obtained from the Alouette II satellite (Hartz, 1970). Both sets of VLF data were taken irrespective of magnetic conditions. In spite of this there is remarkable coincidence between the hiss and the location of the soft zone.

B. Magnetic Effects

The movement of the electrons along the magnetic field lines constitutes electric currents along the field lines. The magnetic effects of such currents should be and are measured by magnetometers flying through the region of the soft zone.

We first consider the transverse magnetic disturbances observed at 1,100 kilometers by magnetometers aboard the satellites 1963-38C and 1964-64A (Zmuda, Armstrong and Heuring, 1970). Magnetic disturbances greater than 30 gammas could be measured by the detectors. Figure 21 contains the boundaries of the quiet time diurnal variation of the magnetic disturbances. The two solid lines are the hourly averages of the upper and lower boundaries respectively, and the dashed line is the average location of the maximum of the disturbance. Quiet conditions were defined by K_p being less than or equal to 2+, whereas the soft zone frequency of occurrence map on which the data are superimposed was compiled from magnetic conditions less than or equal to 2. The coincidence between the regions of magnetic disturbance and particle precipitation is remarkable. Zmuda et al. (1970) have also shown that the average locations of the transverse magnetic disturbances move equatorward slightly less than 2^o per value of K_p, similar to the particle observations. To account for the magnetic disturbances they estimate that the particle fluxes must be between 10^8 and 3.5×10^9 particles/cm^2-sec. As we shall see (Table 1) the intensity of the electron precipitation in the soft zone is sufficient to produce these magnetic fluctuations.

The electron precipitation measurements indicate either spatial or temporal structures often of the order of 1 second or less in extent. The motion of search coil magnetometers through these regions of field aligned currents should produce signals in the few hertz or few tens of hertz frequency range. Such AC magnetic variations are indeed observed as shown in Figure 22. The search coil magnetometer data was also obtained from an experiment aboard OGO-4 (Burton et. al, 1969). The X and Y magnetometers were oriented 45^o and 135^o respectively to the radius vector

from the earth and the Z axis magnetometer made an orthogonal set. They responded primarily to the frequency range around one hz. Field aligned currents at high latitudes where the magnetic field lines are nearly vertical would produce a magnetic field in the horizontal direction, and, therefore, the X and Y magnetometers should show fluctuations exactly in phase and in the same sense. The small variations in the beginning of the figure are due to spacecraft boom vibrations. Exactly in coincidence with the first observation of the electron precipitation the search coil magnetometers showed an increase in the fluctuations. Note throughout the record the phase relation between the X and Y signals. At times the search coil signals were so strong that the signal saturated. This is especially seen from one second to five seconds after 2324 UT. Note at the end of the figure at 2324:05.4 the exact coincidence in cessation of both the particle flux and the search coil magnetometer outputs. Since the magnetic field was apparently not changing outside of the particle beam, this measurement probably indicates the existence of a sheet current with an edge at 2324:05.

C. Electric Effects

Similar to magnetic field effects, electric field probes flying through this region of extremely structured radiation should also measure field fluctuations in the one to several tens of hz range. Such fields could be due to polarization electric fields, the primary field which might possibly cause the field aligned currents, or to electron density irregularities. We show in Figure 23 the locations of the maximums in the 3 to 30 hz irregularity signal from the electric field probe aboard the OV1-10 satellite when $K_p \leq 2$ (Maynard and Heppner, 1970). The data

acquisition from this experiment was not evenly distributed in magnetic local time, causing a lack of observations after midnight and at dusk. Again the maximums of the irregularity signals seem to lie predominantly at latitudes of the soft zone.

D. Ionization Effects

Sato and Collin (1969) have studied electron concentration enhancements from measurements made by the top-side sounder aboard Alouette I at a height of 1000 kilometers at polar latitudes during 1962 to 1964. In an initial analysis of this data, Thomas et al (1966) suggested that these peaks of electron concentrations were due to electrons diffusing upwards along the lines of force to 1,000 kilometers from lower down in the F-region, where they were produced by energetic particles from the magnetosphere which were accelerated along neutral lines and entered the earth's atmosphere.

Sato and Collin plotted the distributions of the locations of electron concentration enhancement peaks for a variety of epochs and magnetic conditions. In order to compare these distributions with the location of the soft zone as defined by the OGO-4 data, we have chosen the November 1962 to January 1963 plot with $K_p \leq 2$. The superposition of these data sets appears in Figure 24. Except for a few scattered points the locations of electron concentration enhancement peaks fall within the soft zone. With an increase in magnetic activity the distribution seemed to spread to both lower and higher latitudes and essentially fill the morning and noon portions of the polar cavity. The spreading to lower latitudes is in agreement with the relationship of the soft zone to K_p, but the soft zone upper boundary usually also moves equatorward with increasing magnetic

activity. However, during substorms electron precipitation has been observed within the polar region, although usually with a slight break in the precipitation pattern to allow for the identification of an upper boundary to the soft zone.

The high altitude ionization from the very soft electron precipitation spectrum is also evident as an anomalously high E-layer. The ionospheric sounder aboard the AFCRL flying ionospheric laboratory measured an E-layer virtual height of about 140 km from 75 to 78 degrees latitude at local noon (Whalen, Buchau, and Wagner, 1971).

The energy input into the soft zone in the form of superthermal charged particles is, of course, highly variable. While the high altitude electron concentration enhancement peaks may be localized because of collimated influx beams, average energy input values may be more appropriate for use in calculating the effects on the ionosphere. The apparent fleeting nature of dayside auroras suggests rather short term beams, so localized effects may become averaged out. We list in Table 1 some average values of particle influx, energy influx and average energies for typical passes of OGO-4 and a single pass of ISIS-1 through the soft zone during low K_p, keeping in mind that the numbers quoted for OGO-4 are based on only a four point spectrum and the "total" values pertain to electrons between 0.7 and 25 keV only. One sees that typically the OGO-4 experiment measured about 10% of the total particle flux, whereas it observed closer to half of the total energy influx. Peak values were roughly ten times these average values for OGO-4 and two to four times for ISIS-1.

E. Dayside Auroral Oval

Auroras in the dayside auroral oval, when observed visually during the winter, appear considerably different in form than auroras observed

during auroral breakup in the midnight region (Figure 25). The dayside auroras are discrete rayed auroral forms as shown in this photograph taken from an airplane by the Air Force Cambridge Research Laboratories (Buchau, private communication, 1971). In movies of all-sky camera pictures of daytime auroras, the forms are very short lived and fleeting. Because they are weak, structured forms, they are usually seen primarily in the zenith; that is, they are extremely aspect sensitive.

We have sought an association between the electron precipitation in the soft zone (daytime portion of the frequency of occurrence map) and optical measurements of the daytime auroras. Many investigators have used all-sky cameras and photometric data to determine the frequency of occurrence of auroral forms at different local times. In order to make a meaningful comparison of any optical data with the frequency of occurrence map we want to choose the optical study which employed procedures most analogous to those we used to compile the map. We considered the published data of Feldstein (1966), Lassen (1969), Sandford (1968), and Stringer and Belon (1967) and determined that the last referenced work was the one most suitable for comparison with the particle precipitation observations (Hoffman and Berko, 1971). Using data acquired by an all-sky camera network based in Alaska during the winter of 1964-65, Stringer and Belon produced contour maps showing the probabilities of observing discrete and homogeneous auroral forms in 15 minute intervals during magnetically quiet periods. It is their isoauroral diagram for discrete auroral forms which we wish to compare with the frequency of occurrence map in the daytime hours, because discrete auroras are the dominant auroral form in these hours and have been used by the previously listed investigators to define the auroral oval in these hours.

In Figure 26 we have shaded the region between 4 and 18 hours local time where the probability of occurrence of the soft zone is greater than at least 50%. The cross-hatched area in these same hours denotes the region of greater than 15% probability of discrete auroral optical emissions presented by Stringer and Belon. The superposition of these two regions during the daytime hours is very apparent. Furthermore, both regions are considerably broader in latitude during the pre-noon hours than the afternoon hours.

It has been shown previously that there is sufficient energy in the more intense structures in the dayside soft zone to produce auroras visible on all-sky-camera photographs (Hoffman and Berko, 1971).

Photometric measurements of dominant auroral emission lines, taken especially from aircraft in the daytime hours, clearly display the effects of the soft radiation on the optical emissions. On the basis of 5 flights through the daytime hour auroral regions, Eather and Mende (1971) have plotted the average ratio of the 6300 OI/4278 N_2^+ as a function of invariant latitude (Figure 27). The ratio goes from a low typical nighttime value between 70 and 75 degrees to the very large ratio at the three points plotted at 79, 81 and 83 degrees invariant latitude. This large ratio is caused, of course, by the fact that the soft zone spectrum produces excitations at high altitudes where the λ6300 oxygen emission predominates.

PART III. EFFECT OF MORNING HARD ZONE PRECIPITATION

A. Absorption Events

The analysis of energetic electron data (≥ 50 keV energy) has clearly shown that these electrons are injected into the trapping region in the restricted local time sector near midnight during substorms. The electron

groups are then observed to move eastward about the earth with a mean speed, velocity dispersion and change in profile characteristic of gradient and curvature drift motion in the distorted dipole field, (Arnoldy and Chan, 1969; Pfitzer and Winckler, 1969; Lezniak and Winckler, 1970). Other observations have shown a very close correlation between the appearance of electron increases at synchronous orbit and the precipitation of electrons into the atmosphere which are detected as auroral x-rays by balloon instrumentation (Parks and Winckler, 1968). One is lead to the conclusion that the injection of these electrons in the midnight sector during substorms is accompanied by simultaneous scattering and precipitation into the atmosphere as these electrons drift eastward in longitude. One should expect then that the zone of precipitation and ionization in the ionosphere should also sweep eastward around the earth. To study this question, Rosen and Winckler (1970) analyzed data from the Alaskan chain of riometers operated by ESSA. This series of seven instruments covered the range of L-values from 3.9 to 8.0.

When examining substorm absorption events recorded by the stations of the riometer chain, it was observed that the absorption did not always begin simultaneously at all stations. Instead the onset progressed either northward or southward along the chain. If the chain of stations was located in the morning hours and a substorm occurred in the midnight region, where a body of electrons would be injected onto close field lines, one would expect the precipitation and, therefore, the riometer absorption, to be measured first at high L-values or high invariant latitudes with a progression of absorption onsets toward low values. This is because the drift rate at higher L-values is faster than at lower L-values, and in fact it is roughly linear with the L-value. Therefore, the lag time

to the onset of the event should be longer at the low L-value stations than at the high L-value stations. Rosen and Winckler normalized these lag times to L-values of 3.9 and 8 and plotted the difference in the lag times for the L-values as a function of the local time of the stations at the onset of the storm (Figure 28). Both positive and negative lags were seen around midnight but the average lag shifted with local time toward a predominantly positive value. This means that the electrons at low L-values did indeed take longer to arrive at the local time of the chain of stations than the electrons at the higher L-values. Assuming that these precipitating electrons had energies of 50 kilovolts during their drift times, the lag difference is given by the solid line labeled 50 kilovolts in the figure. This agrees with the average measured lag times from 0 hours to 12 hours local time. The 50 kilovolt electrons have the correct energy to produce the ionization in the D-region to cause riometer absorption, because their maximum ionization rate occurs at an altitude of 90 kilometers.

It is well known that most of the energy precipitating into the atmosphere in the midnight hours during a substorm is carried by electrons having energies in the few kilovolt range rather than at 50 kilovolts. In light of the morphology of these 50 kilovolt electrons one then asks what happens to the kilovolt electrons after a substorm. We have evidence that these electrons also drift in local time through the morning hours and precipitate to form the hard zone (Hoffman, 1970). An example of such a precipitation event in the morning hours is shown in Figure 29. A substorm occurred around 1200 UT as seen in the College magnetogram, followed by a small disturbance noted especially at Chelyuskin from 1700 to

almost 2100 hours UT. A series of four late morning satellite passes occurred between 18 hours and 23 UT. In the top of the figure, the first, third, fourth, and fifth panels show the 7.3 keV precipitation at about 10 hours magnetic local time. In the first panel of data which occurs during the small disturbance at Chelyuskin, only the high latitude portion of the hard zone is seen. On Revolutions 1243, 1244, and 1245, the latter two after all activity had ceased in the midnight region, the hard zone is clearly observed. Instead of requiring only from tens of minutes to an hour for these electrons to drift from midnight to noon, drift times are measured in several hours. Thus following a substorm, if this interpretation is correct, the hard (> 50 keV) electrons will precipitate first at a morning hour station and the average energy of the precipitation will slowly soften as a function of time. The morphology of ionization over a ground station situated in the morning hours is complicated by the fact that the initial ionization is produced some tens of minutes after the onset of a substorm in the D-region. Then there should be a very slow transition over a period of several hours, during which time the station would move to later morning hours, to a more typical E-layer absorption event from the hard zone electrons.

B. Auroral Events

In Part II of this review we associated the soft zone electron precipitation with the daytime portion of the auroral oval. We also saw in Part I that the hard zone was situated immediately on the low latitude side of the soft zone. Since the energy spectrum of precipitating electrons in the hard zone is typically shaped like the spectrums in the midnight

regions, it would be expected that auroral phenomena produced by these electrons in the morning hours would be dominated by the more typical auroral emission features that one finds in the midnight region.

In searching for an auroral optical phenomenon which could be associated with the hard zone, we found that the auroral type defined as the "mantle aurora" by Sandford (1968) is consonant with our particle observations (Hoffman, 1970). This aurora, measured photometrically at the λ3914 and λ5577 emissions, is a relatively steady, diffuse, subvisual aurora covering a large area of the sky, and occurring in the absence of discrete auroral forms as recorded on ground level all-sky camera photographs (Gowell and Akasofu, 1969). Sandford (1968) found that on integrating the emissions over the entire high latitude region, the mantle auroral emissions were on the average the predominant optical phenomenon during solar maximum, giving rise to the majority of all auroral emissions, while at solar minimum such emissions dropped to about half the emissions. This suggests that the mantle aurora region of space is an important sink for energy from the magnetosphere.

Under the assumption that the precipitating electrons were isotropic over the upper hemisphere at all energies, three typical energy spectrums of the energy influx are shown in Figure 30. Note that energy is carried into the atmosphere at energies all the way up at least 25 kilovolts. Rees (1970) calculated the column emission rates for λ3914, λ5577 and λ6300 from the spectrum shown in Figure 30, marked Revolution 1108. Assuming the energy spectrums of precipitation events in the hard zone are consistently shaped like spectrum 1108 in Figure 30, the flux of 10^6 electrons/cm^2-sec-ster at 7.3 keV, which was used to define the boundaries of the

hard zone in Figure 15, would correspond to the energy influx which would produce 0.25 kR contours of λ3914 emissions.

Sandford (1968; Figure 3) published contours of this emission from data obtained by photometric methods in the sourthern hemisphere. We compare this 0.25 kR contour as well as the 0.5 kR contour with the region of 7.3 keV electron precipitation in Figure 31. At higher latitudes we also show the location of the auroral oval as defined by Stringer and Belon (1967) with the same contour that appears in Figure 26. All data in the figure are compiled irrespective of K_p. The coincidence between the 7.3 keV electron precipitation region and the λ3914 emission region is not exact. However, note from 05 through 11 hours MLT the strikingly identical shift in the boundary locations with respect to MLT, particularly between the particles and the 0.5 kR contour. Also note that the optical emissions decrease in intensity in the late morning hours, especially where the 7.3 keV precipitation region seems to end. Certainly there is no relationship between the 7.3 keV precipitation and the auroral oval in the morning hours. Exact agreement would not be expected between the electron precipitation and λ3914 emission regions because the optical data were acquired during the southern winter of 1963, whereas the particle measurements were made during the last half of 1967 and the beginning of 1968. In addition criteria established to define the respective boundaries are not necessarily entirely compatible. No relationship between particle precipitation and Sandford's contours in the nighttime hours has been established. The general coincidence in the afternoon hours between Stringer and Belon's auroral occurrence contours for discrete aurora and Sandford's λ3914 emission contours during periods of no discrete aurora also is not understood.

On the basis of the following facts: (1) that the electron energy influx is sufficiently intense and has the proper spectrum to produce the optical emissions which Sandford has defined as the mantle aurora; (2) the regions of precipitation and light emissions are reasonably associated spatially; and (3) both the electron influx and the optical emissions are diffuse in nature, we concluded that the precipitation of these drifting electrons, apparently originating near midnight during substorms, is the cause of the mantle aurora (Hoffman, 1970).

CONCLUDING REMARKS

In this review we have attempted to collect and integrate the various low energy charged particle measurements from satellites in the dawn and dayside hours of the polar domain, and to present some of the properties of the particles observed in this region. It is obvious that only the grossest characteristics of the radiation have been investigated, but hopefully the material presented here will be a base from which more definitive studies can originate. The thorough analysis of specific events as well as more careful statistical studies of the collective behavior of these particles are required, utilizing larger data bases and additional, more physically meaningful supporting data, in order to understand the origin, history, and control of these particles.

If indeed the soft zone electrons are the result of the penetration of the magnetosheath plasma through the dayside magnetospheric cusps or "neutral points", specific relations between the location of the soft zone, the magnetospheric configuration and interplanetary conditions should exist. At first glance it appears that, in addition to field line interconnection between the magnetosphere and the magnetosheath, the particles must experience interactions within the magnetosphere in order to account for the spectral shapes, pitch angle distributions (Hoffman and Evans, 1968) and the structure of the radiation, which rapidly vary with space or time, and the apparent overlap of the soft zone with closed field lines.

We have not specifically addressed the question of how far the soft zone extends into the nighttime hours, or what relationship might exist between the low energy, structured precipitation during magnetically quiet periods in the nighttime hours with the soft zone.

The temporal history of the hard zone in the morning hours requires considerably more analysis. We have not been able to find any analysis of ground based observations relating to the effects of less than 50 keV precipitation in the hard zone which considered the possibility that the source of particles drifted in local time. Perhaps the most definitive studies of drifting electron clouds must be performed from equatorially stationed satellites. The synchronous orbit is at too small an L value ($\Lambda = 67^{\circ}$) to measure events throughout the hard zone, and may be applicable only to the midnight region and the lower portion of the hard zone. Note on Figure 31 that the hard zone shifts to latitudes higher than 67° at about 06 hours MLT on the average. Hopefully, data already acquired from such satellites will be able to illuminate the particle precipitation mechanism.

The observation of a large number of geophysical phenomena at high latitudes on the dayside of the dipole have been published, but there is only beginning a realization that they probably have a common relationship with the electrons precipitating in the soft zone. For this reason we attempted to compile as many phenomena as possible which seem to have this common origin. We wish to point out that in those figures which contain the superposition of soft zone phenomena on the rectilinear simplified probability map of the 0.7 keV structured electron precipitation, only the spatial relationship of the phenomena to the soft zone in the daytime hours is being considered.

The direct cause and effect relationships between the precipitating electrons and each of the individual phenomena have only begun to be investigated. For each type of event a host of questions remain to be answered.

• It is necessary to calculate from a well measured electron spectrum the total power produced via the Cerenkov process, to compare with the measured strength of the VLF auroral hiss. Further details of the electromagnetic radiation must be investigated, especially the effect of the ionosphere on the propagation of the hiss. This is possibly an area rich in wave-plasma phenomena.

• While the soft zone precipitation seems to consitute field aligned currents, the total current system, and its relation to the magnetospheric configuration is still unknown. Since the types of ionospheric as well as magnetospheric currents which flow in the dayside ionosphere have not been determined we have intentionally ignored the large body of ground based magnetic measurements from these hours.

• The interaction of the soft zone electrons with the dayside ionosphere will be extremely difficult to study because of the great spatial gradients or rapid temporal variations which exist in the energy source and, therefore, the extremely localized and perhaps transient effects on the ionosphere. This is a region which has been almost totally ignored by investigators utilizing sounding rockets.

• While we believe that there is no direct relationship between the existence of the dayside portion of the auroral oval and the nighttime portion, and, therefore, there are two major independent sources for auroral particles, the boundary conditions between these regions are not defined. The entire subject of polar cap auroras and the existence of the winter ionosphere has been neglected.

A large body of data from numerous experiments and satellites as well as associated ground observations now exist which certainly bear on these problems. These data together with the increasing awareness of the interrelationships between the variety of phenomena which exist in the dawn and dayside hours should enable a large number of these problems to be studied in depth in the succeeding years.

ACKNOWLEDGMENTS

In the preparation of the material for this review, we wish to thank Mr. F. W. Berko for his participation in data analysis, Mr. R. W. Janetzke for data display support, Mr. R. D. Gribble for illustrations, and Mrs. Anne Thompson for her able assistance and patience in preparing and repeatedly revising the manuscript.

I spent an interesting and fruitful day learning about dayside optical and ionospheric measurements with Messrs. J. Buchau, J. A. Whalen, C. P. Pike, and Mrs. R. A. Wagner at AFCRL, and appreciate their permission to reproduce the dayside aurora photograph. Professor R. E. Holzer and Mr. R. K. Burton have kindly allowed the publication of their search coil magnetometer data while we are engaged in a joint analysis project. Also I am grateful to Professor T. Laaspere for his permission to use his OGO-4 VLF data while we are preparing a joint publication. Mr. J. D. Winningham has kindly allowed me the use of data from his very timely thesis. Quite a number of authors have granted permission to use their published data.

I wish to also thank Drs. T. A. Fritz and S. J. Bauer for helpful discussions.

REFERENCES

Archuleta, R. J., and DeForest, S. E., 1971. Efficiency of channel electron multipliers for electrons of 1-50 kev. Rev. Sci. Instru., 42, 89-91.

Arnoldy, R. L., and Chan, K. W., 1969. Particle substorms observed at the geostationary orbit. J. Geophys. Res., 74, 5019-5028.

Burch, J. T., 1968. Low-energy electron fluxes at latitudes above the auroral zone. J. Geophys. Res., 73, 3585-3591.

Burton, R. K., Holzer, R. E., and Smith, E. J., April 1969. Intense magnetic impulses and chorus observed in the auroral zone during particle precipitation. (Abstract) American Geophysical Union, Wash., D. C.

Cummings, W. D., Barfield, J. N., and Coleman, P. J., 1968. Magnetospheric substorms observed at the synchronous orbit. J. Geophys. Res., 73, 6687-6698.

Eather, R. H., and Mende, S. B., 1971. Airborne observations of auroral precipitation patterns. J. Geophys. Res., 76, 1746-1755.

Fairfield, D. H., 1968. The average magnetic field configuration of the outer magnetosphere. J. Geophys. Res., 73, 7329-7338.

Feldstein, Y. I., 1966. Peculiarities in the auroral distribution and magnetic disturbance distribution in high latitudes caused by the asymmetrical form of the magnetosphere. Planet. Space Sci., 14, 121-130.

Frank, L. A., 1970. Plasma in the earth's polar magnetosphere. Preprint 70-55, Dept. of Physics and Astronomy, The University of Iowa.

Gowell, R. W., and Akasofu, S.-I., 1969. Irregular pulsations of the morning sky brightness. Planet. Space Sci., 17, 289-290.

Hartz, T. R., 1970. Low frequency noise emissions and their significance for energetic particle processes in the polar magnetosphere. The Polar Ionosphere and Magnetospheric Processes, ed. G. Scovli, Gordon and Breach, New York.

Heikkila, W. J., and Winningham, J. D., 1971. Penetration of magnetosheath plasma to low altitudes through the dayside magnetospheric cusps. J. Geophys. Res., 76, 883-891.

Hoffman, R. A., 1969. Low-energy electron precipitation at high latitudes. J. Geophys. Res., 74, 2425-2432.

Hoffman, R. A., June 1970. Auroral electron drift and precipitation: cause of the mantle aurora. Goddard preprint, X-646-70-205 (submitted to J. Geophys. Res.).

Hoffman, R. A., and Berko, F. W., 1971a. On the dual nature of the auroral oval. Abstract, American Geophysical Union, April 12-16, 1971, Wash., D.C.

Hoffman, R. A., and Berko, F. W., 1971. Primary electron influx to the dayside auroral oval. J. Geophys. Res., 76, 2967-2976.

Hoffman, R. A., and Evans, D. S., 1968. Field-aligned electron bursts at high latitudes observed by OGO 4. J. Geophys. Res., 73, 6201-6214.

Jørgensen, T. S., 1968. Interpretation of auroral hiss measured on OGO-2 and at Byrd Station in terms of incoherent Cerenkov radiation. J. Geophys. Res., 73, 1055-1069.

Lassen, K., 1969. Polar cap emissions. Atmospheric Emissions, ed. B. M. McCormac and A. Omholt, Van Nostrand Reinhold Co., New York, p. 63-71.

Laaspere, T., and Hoffman, R. A., June 1971. A comparison of VLF auroral hiss with precipitating low-energy electrons using simultaneous data from two OGO-4 experiments. (Abstract) COSPAR, Seattle.

Laaspere, T., Johnson, W. C., and Semprebon, L. C., 1970. Observations of electric fields in the frequency range 20 Hz - 540 kHz on OGO-6. Symposium on Upper Atmospheric Currents and Electric Fields, Boulder, Aug. 1970.

Lesniak, T. W., and Winckler, J. R., 1970. An experimental study of magnetospheric motions and the acceleration of energetic electrons during substorms. J. Geophys. Res., 75, 7075-7098.

Maehlum, B. N., 1968. Universal-time control of the low-energy electron fluxes in the polar regions. J. Geophys. Res., 73, 3459-3468.

Maehlum, B. N., 1969. On the high latitude, universal time controlled F-layer. J.A.T.P., 31, 531-538.

Maynard, N. C. and Heppner, J. P., 1970. Variations in electric fields from polar orbiting satellites. Particles and Fields in the Magnetosphere, ed. B. M. McCormac, Reinhold Pub. Co., New York, 247-253.

Parks, G. K., and Winckler, J. R., 1968. Acceleration of energetic electrons at the synchronous altitude during magnetospheric substorms. J. Geophys. Res., 73, 5786-5791.

Paschmann, G., Shelley, E. G, Chappell, C. R., Sharp, R. D. and Smith, L. F., 1970. Absolute efficiency measurements for channel electron multipliers utilizing a unique electron source. Preprint, Lockheed Palo Alto Research Laboratory, Palo Alto.

Pfitzer, K. A., and Winckler, J. R., 1969. Intensity correlations and substorm electron drift effects in the outer radiation belt measured with the OGO-3 and ATS-1 satellites. J. Geophys. Res., 74, 5005-5018.

Rees, M. H., 1970. Effects of low energy electron precipitation on the upper atmosphere. The Polar Ionosphere and Magnetospheric Processes, ed. G. Scovli, Gordon and Breach, New York.

Rosen, L. H., and Winckler, J. R., 1970. Evidence for the large-scale asimuthal drift of electron precipitation during magnetospheric substorms. J. Geophys. Res., 75, 5576-5581.

Sandford, B. P., 1968. Variations of auroral emissions with time magnetic activity, and the solar cycle. J. Atmos. Terr. Phys., 30, 1921-1942.

Sato, T., and Colin, L., 1969. Morphology of electron concentration enhancements at a height of 1000 kilometers at polar latitudes. J. Geophys. Res., 74, 2193-2207.

Sharp, R. D., and Johnson, R. G., 1968. Satellite measurements of auroral particle precipitation. Earth's Particles and Fields, ed. B. M. McCormac, Reinhold Pub. Corp., New York.

Stringer, W. J., and Belon, A. E., 1967. The morphology of the IQSY auroral oval: 1. Interpretation of isoauroral diagrams. J. Geophys. Res., 72, 4415-4421.

Thomas, J. O., Rycroft, M. J. Colin, L., and Chan, K. L., 1966. The topside ionosphere, II. Experimental results from the Alouette I satellite. Electron Density Profiles in Ionosphere and Exosphere, ed. J. Frihagen, p. 322-357, North-Holland Pub. Co., Amsterdam.

Vernov, S. N., Melnikov, V. V., Savenko, I. A., and Savin, B. I., 1966. Measurements of low-energy particle fluxes from the Cosmos and Electron satellites. Space Res. VI, 746-756.

Whalen, J. A., Buchau, J., and Wagner, R. A., 1971. Airborne ionospheric and optical measurements of noontime aurora, J. Atmos. Terr. Phys., 33, 661-678.

Winningham, J. D., 1970. Penetration of magnetosheath plasma to low altitudes through the dayside magnetospheric cusps. Ph.D. Thesis, Texas A&M University, Dec. 1970.

Zmuda, A. J., Armstrong, J. C. and Heuring, F. T., 1970. Characteristics of transverse magnetic disturbances observed at 1100 kilometers in the auroral oval. J. Geophys. Res., 75, 4757-4762.

TABLE 1

	Total Flux Precipitated	Total Energy Precipitated	Average Energy
OGO-4 Morning	2-3 x 10^8	0.3	1.3
OGO-4 Afternoon	1 x 10^8	0.1	0.9
ISIS-1 Noon (1)	3 x 10^9	0.5	

Total Flux in electrons/cm^2-sec

Total Energy in ergs/cm^2-sec

Average Energy in keV

(1) Heikkila and Winningham (1971)

FIGURE CAPTIONS

Figure 1. The dayside zones of precipitation identified by charged particle detectors flown on low altitude polar satellites (Sharp and Johnson, 1968).

Figure 2 The hard (auroral) zone and soft zone at magnetic local noon as measured by the Aurora-1 satellite (Burch, 1968).

Figure 3. Data from the Auroral Particles Experiment on OGO-4 during a pass in the northern hemisphere from dusk-to-dawn. K_p was 0+. The two detectors at 0.7 keV and 7.3 keV measured electrons with pitch angles near 0^o in an energy band +18%, - 13% about the center energy listed. The counting rate profiles are used to show the existence of the soft zone in the afternoon and morning hours and the hard zone only in the morning.

Figure 4. A late morning hour pass from the OGO-4 satellite revealing the hard and soft regions of precipitation as well as the polar cavity. K_p was 4- during this pass.

Figure 5. Data from the ISIS-1 satellite at local magnetic noon on February 3, 1969. The top portion of the figure contains a spectrogram from precipitating electrons where the density of the trace qualitatively indicates the spectral energy density as a function of particle energy. The middle frame contains the total integrated number flux and the bottom frame contains the total integrated energy flux. K_p during the pass was 4 (Heikkila and Winningham, 1971).

Figure 6. Typical energy spectrums obtained in the soft zone from three different experiments The published Aurora-1 data (Burch, 1968) were based upon efficiencies by Frank and have been modified to agree with the Arnoldy efficiencies for energies above 0.5 keV (Archuleta and DeForest, 1971; Paschmann et al., 1970). The ISIS-1 spectrum is relative only (Heikkila and Winningham, 1971).

Figure 7. Electron spectrums in the hard zone from Aurora-1 and OGO-4. The Aurora-1 data have again been modified for channel electron multiplier efficiencies.

Figure 8. Soft zone frequency of occurrence map for $K_p \leq 2$ based on OGO-4 data in an invariant latitude magnetic local time coordinate system (Hoffman and Berko, 1971).

Figure 9. The OGO-4 soft zone with the location of the soft zone on the dayside as defined by data from ISIS-I and Aurora 1 superimposed.

Figure 10. The latitudes of the high and low latitude boundaries of the soft zone from OGO-4 near local noon for two different epochs plotted as a function of K_p. The top two panels contain all the data points whereas the bottom two panels contain averages over each integral value of K_p.

Figure 11. The upper boundary and lower boundary of the soft zone for magnetic quiet periods as a function of UT. In the top figure the solid dots were obtained from the Aurora-1 satellite (Maehlum, 1968). The numbers by some Aurora-1 data points are K_p during the time of the boundary acquisition.

Figure 12. The latitude of the upper boundary of the soft zone at noon when $K_p \leq 1+$ as a function of β, the angle between dipole axis projected onto the noon-midnight meridian plane and the earth-sun line.

Figure 13. The location of the dayside soft zone as defined by precipitating protons as a function of K_p. The data were obtained from Winningham (1970). The geomagnetic tilt angle β is indicated by each data point.

Figure 14. Data from an OGO-4 satellite pass acquired near midnight during a substorm when K_p was 5. See Figure 3 caption for a description of the detector.

Figure 15. The hourly average location of the hard zone as defined by the 7.3 keV detector on OGO-4 as a function of magnetic local time irrespective of magnetic activity. The mean deviations of the boundary locations are slightly less than 2^o at each hour.

Figure 16. The average ratio of 0.7 keV to 7.3 keV fluxes at three different local times as a function of invariant latitude.

Figure 17. Simultaneous measurements of VLF auroral hiss and 0.7 keV precipitating electrons by the OGO-4 satellite. The bandpass of the VLF experiment which used an electric dipole antenna was 100 hz to 18 khz. The logarithm of the flux at 0.7 keV is plotted. The soft zone begins at about 1844:45 U.T. for the November 12 event and at 2150:33 for the November 14 event.

Figure 18. Simultaneous measurement of auroral hiss and precipitating electrons with energies around 2.3 and 7.3 keV. The hard zone extends from about 2149:52 to 2150:28 U.T.

Figure 19. An exact correlation between auroral hiss and 0.7 kev electron precipitation at 1112:39 U.T.

Figure 20. The general relationship between VLF auroral hiss measured by electric dipole experiments aboard the OGO-6 (Laaspere, 1971) and Alouette II (Hartz, 1970) satellites and the precipitation of structured 0.7 keV electrons.

Figure 21. The relationship between the average locations of transverse magnetic disturbances greater than 30γ at 1100 km altitude (Zmuda et al, 1970) and the precipitation of structured, 0.7 keV electrons. The magnetic data were compiled when $K_p \leq 2+$ and the particle data when $K_p \leq 2$. Note that most of the measurements of the magnetic disturbances occurred in the daytime hours in the lower portion of the soft zone.

Figure 22. Detailed association between AC magnetic variations (Holzer and Burton, private communication) and 0.7 keV electron precipitation from experiments on OGO-4. The frequency response of the search coil magnetometers had a maximum at 1 hz.

Figure 23. The relationship between maximums in the 3 to 30 hz irregularity signal from the OV 1-10 satellite electric field antennas in early 1967 (Maynard and Heppner, 1970) and the precipitation of structured 0.7 keV electrons. Both sets of data were acquired when $K_p \leq 2$.

Figure 24. The association between electron concentration enhancement peaks measured by the top-side sounder aboard Alouette I at a height of 1000 km from November 1962 through January 1963 (Sato and Collin, 1969) and the precipitation of structured 0.7 keV electrons. Both sets of data were acquired when $K_p \leq 2$.

Figure 25. All-sky-camera photograph of auroras at high latitude on the dayside of the dipole during winter (J. Buchau, private communication).

Figure 26. A polar plot in invariant latitude-magnetic local time of the high probability of structured 0.7 keV electron precipitation during the dayside hours in comparison with the region of high probability of discrete auroras (Stringer and Belon, 1967).

Figure 27. The average ratio of 6300 O I/4278 N_2^+ auroral emissions as a function of invariant latitude for nighttime and daytime (Eather and Mende, 1971).

Figure 28. The effective lag of the starting time of riometer events associated with substorms normalized to an L difference of 8.0 to 3.9 as a function of local time. The histogram represents the average effective lag during 2-hour intervals of local time. The lines labeled 50 keV and 100 keV are theoretical predictions of drift times from midnight in a dipole field for electrons of the listed energies.

Figure 29. Evidence for drift of low energy electrons on closed field lines from the midnight region through the morning hours. The M on the magnetograms denotes the time the observatory passed magnetic midnight. The precipitation during revolutions 1244 and 1245 at about 09 hours MLT occurred after the magnetic activity in the region of midnight had ceased.

Figure 30. Typical energy spectrums of the energy influx to the hard zone in the morning hours.

Figure 31. A comparison of the region of 7.3 keV electron precipitation, which defines the hard zone and regions of optical emissions. The dashed contours are kR of λ3914 emissions in the absence of discrete auroras in 1963 in the southern hemisphere (Sandford, 1968). The shaded area shows the location of the auroral oval during the morning and daytime hours as defined by Stringer and Belon (1967).

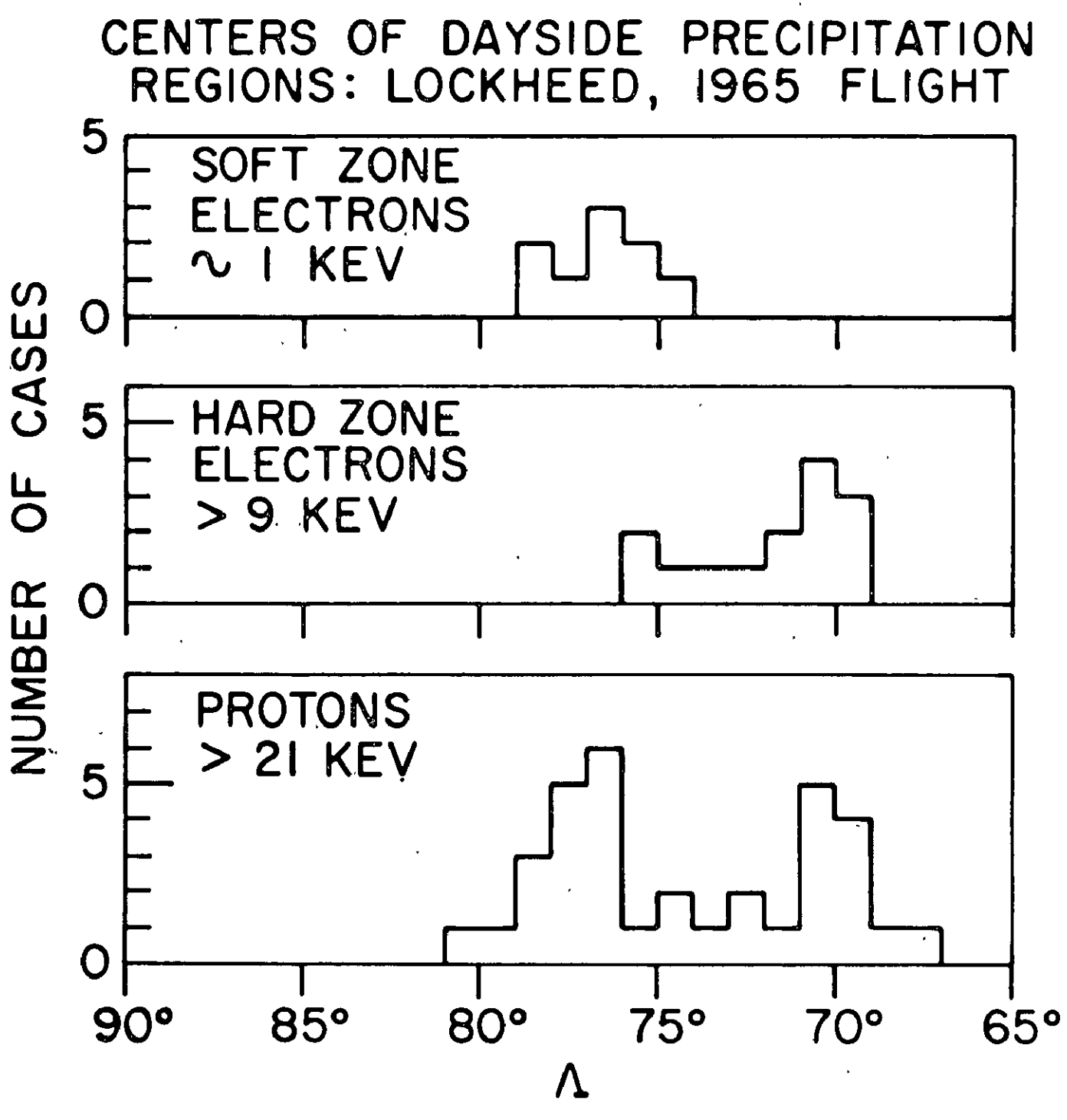
CENTERS OF DAYSIDE PRECIPITATION REGIONS: LOCKHEED, 1965 FLIGHT
SOFT ZONE ELECTRONS ~ 1 KEV
HARD ZONE ELECTRONS > 9 KEV
PROTONS > 21 KEV
NUMBER OF CASES
5
0
90°
85°
80°
75°
70°
65°
Λ

FIGURE 1

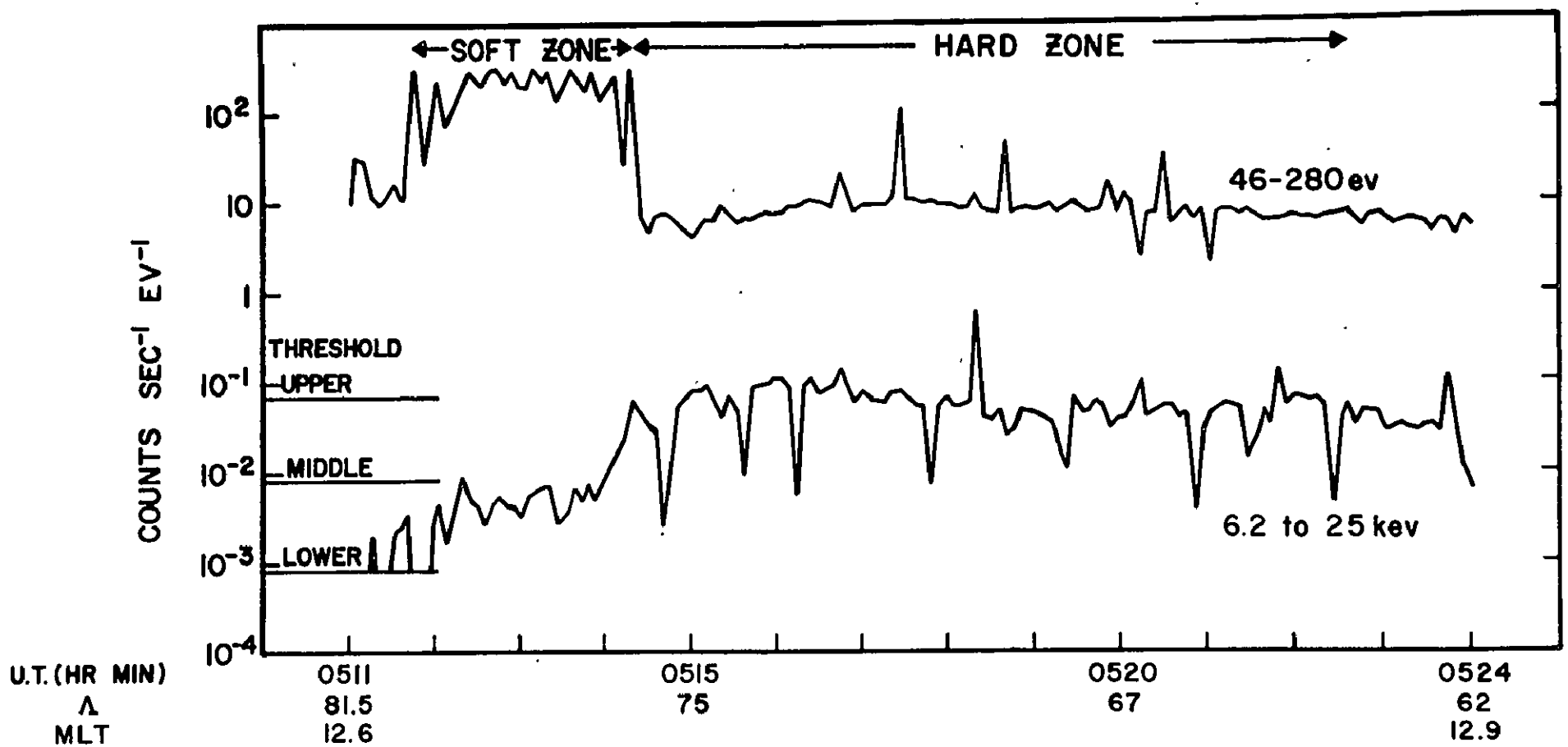
SOFT ZONE
HARD ZONE
46-280ev
6.2 to 25 kev
THRESHOLD
UPPER
MIDDLE
LOWER
COUNTS SEC⁻¹ EV⁻¹
10²
10
1
10⁻¹
10⁻²
10⁻³
10⁻⁴
U.T. (HR MIN)
Λ
MLT
0511
81.5
12.6
0515
75
0520
67
0524
62
12.9

FIGURE 2

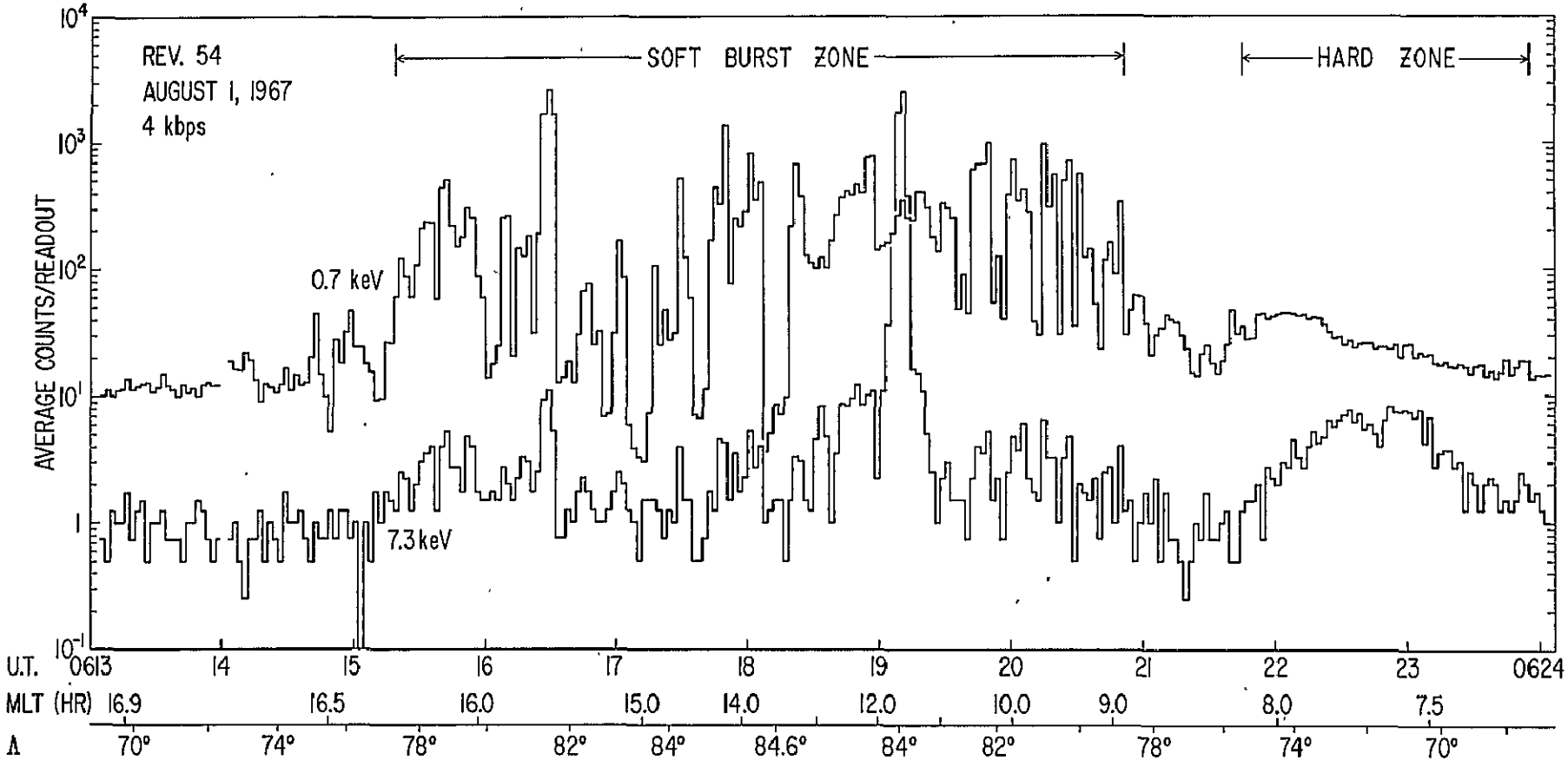
REV. 54
AUGUST 1, 1967
4 kbps
SOFT BURST ZONE
HARD ZONE
AVERAGE COUNTS/READOUT
10^4
10^3
10^2
10^1
1
10^{-1}
0.7 keV
7.3 keV
U.T. 0613 14 15 16 17 18 19 20 21 22 23 0624
MLT (HR) 16.9 16.5 16.0 15.0 14.0 12.0 10.0 9.0 8.0 7.5
Λ 70° 74° 78° 82° 84° 84.6° 84° 82° 78° 74° 70°

FIGURE 3

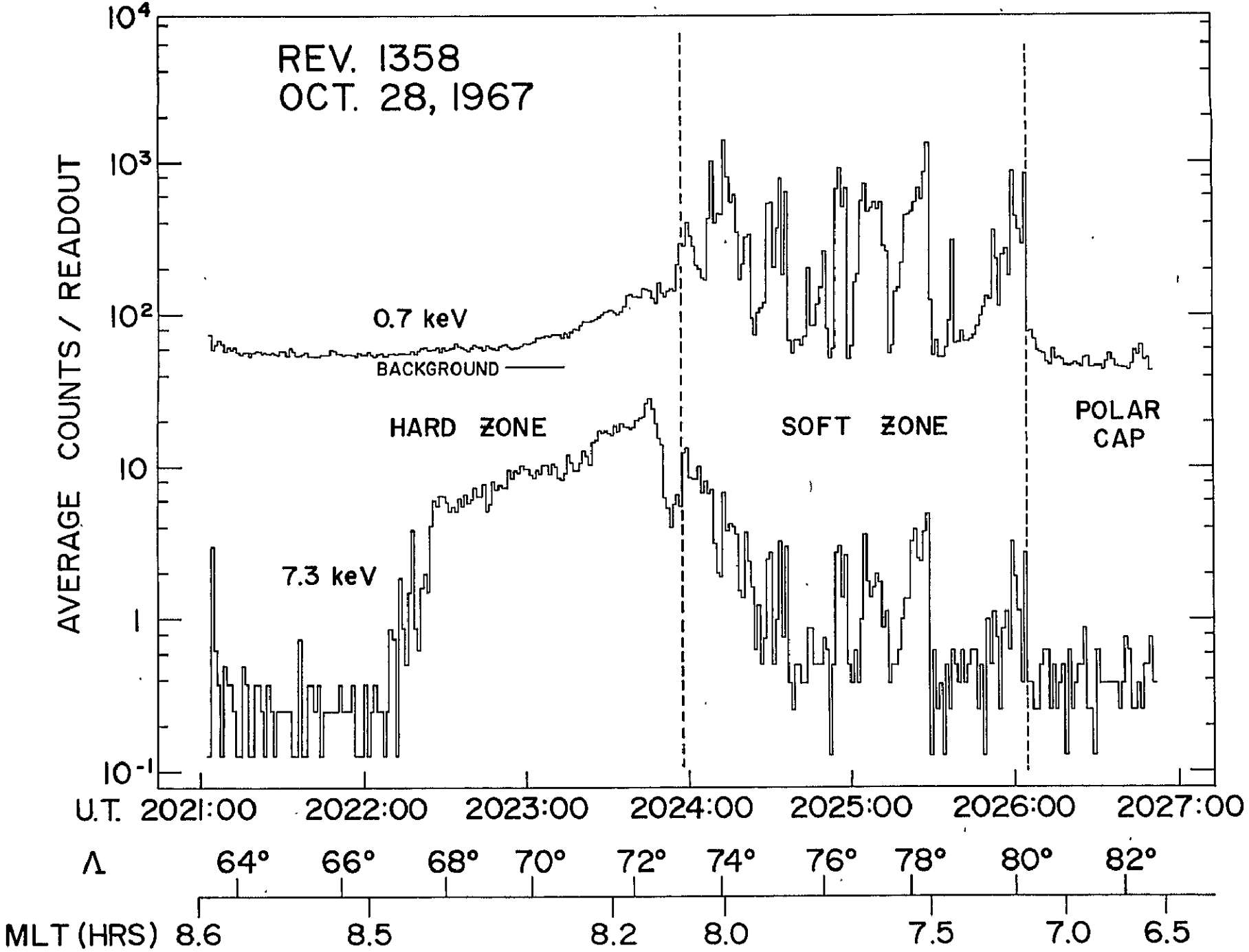
REV. 1358
OCT. 28, 1967
AVERAGE COUNTS / READOUT
10^4
10^3
10^2
10
1
10^{-1}
0.7 keV
BACKGROUND
7.3 keV
HARD ZONE
SOFT ZONE
POLAR CAP
U.T. 2021:00
2022:00
2023:00
2024:00
2025:00
2026:00
2027:00
Λ
64°
66°
68°
70°
72°
74°
76°
78°
80°
82°
MLT (HRS)
8.6
8.5
8.2
8.0
7.5
7.0
6.5

FIGURE 4

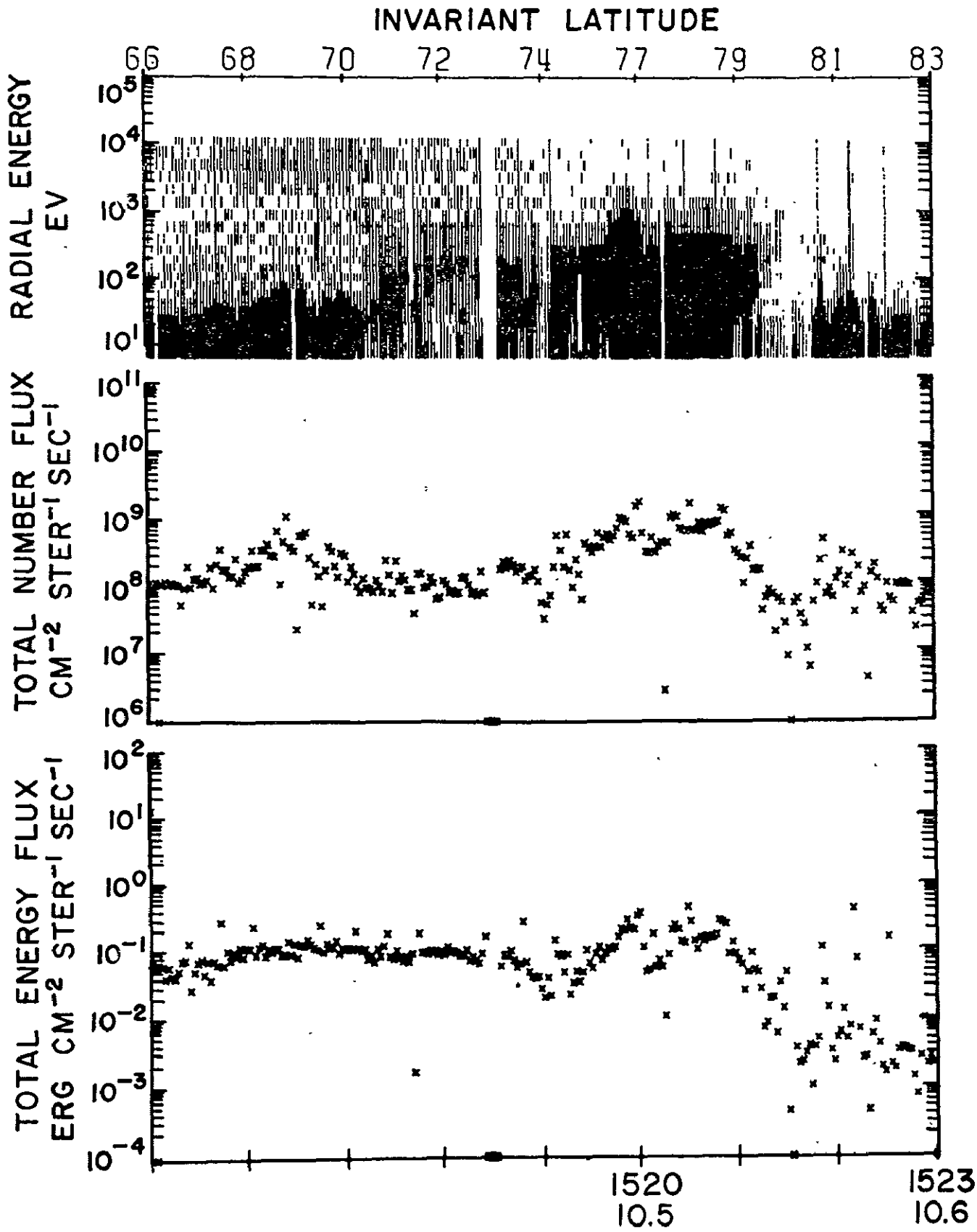
INVARIANT LATITUDE
66
68
70
72
74
77
79
81
83
RADIAL ENERGY
EV
10^5
10^4
10^3
10^2
10^1
TOTAL NUMBER FLUX
CM^{-2} $STER^{-1}$ SEC^{-1}
10^{11}
10^{10}
10^9
10^8
10^7
10^6
TOTAL ENERGY FLUX
ERG CM^{-2} $STER^{-1}$ SEC^{-1}
10^2
10^1
10^0
10^{-1}
10^{-2}
10^{-3}
10^{-4}
1520
10.5
1523
10.6

FIGURE 5

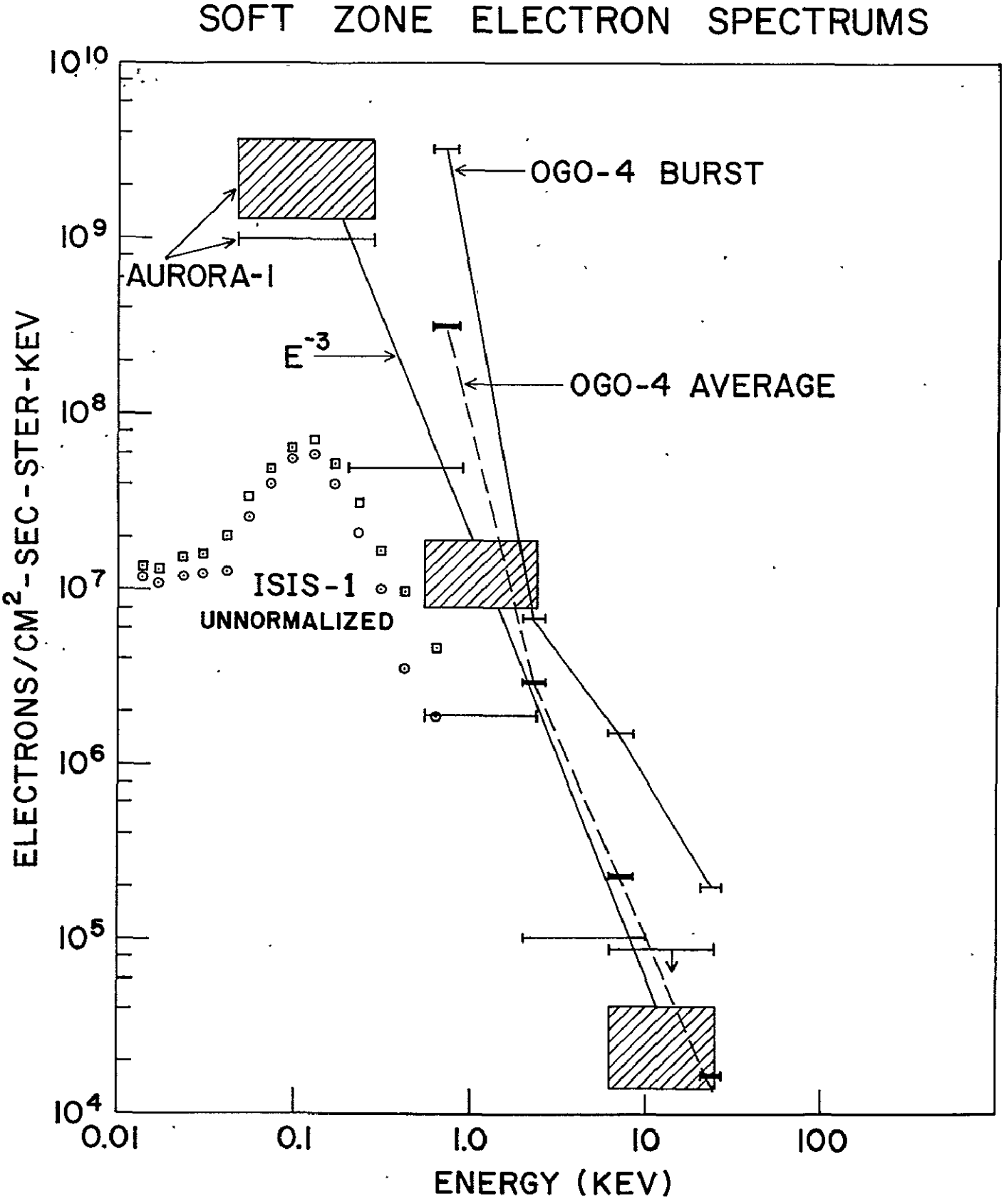
SOFT ZONE ELECTRON SPECTRUMS
OGO-4 BURST
AURORA-1
E^-3
OGO-4 AVERAGE
ISIS-1
UNNORMALIZED
ELECTRONS/CM^2-SEC-STER-KEV
ENERGY (KEV)
10^10
10^9
10^8
10^7
10^6
10^5
10^4
0.01
0.1
1.0
10
100

FIGURE 6

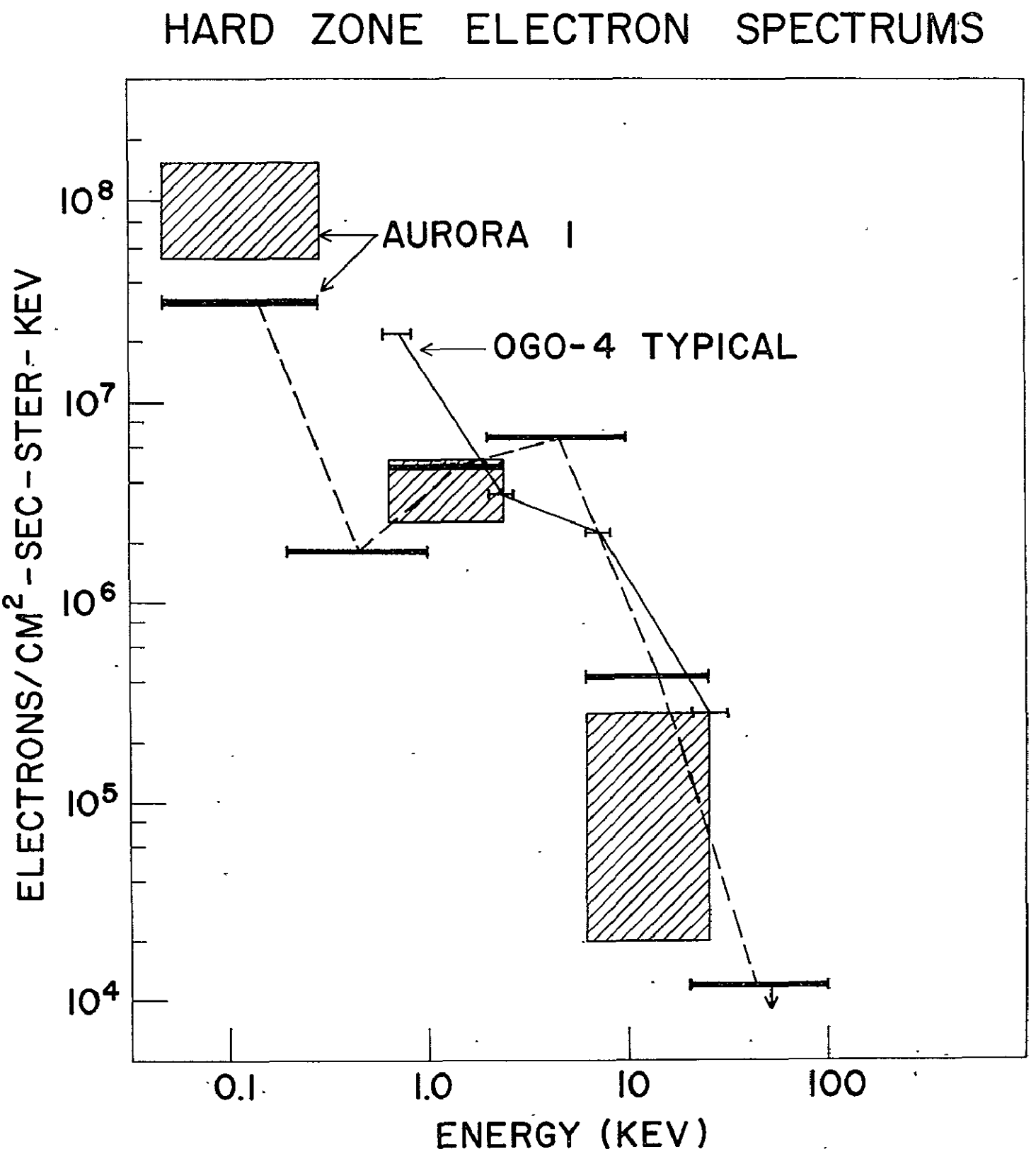
HARD ZONE ELECTRON SPECTRUMS
AURORA I
OGO-4 TYPICAL
ELECTRONS/CM²-SEC-STER-KEV
10⁸
10⁷
10⁶
10⁵
10⁴
0.1
1.0
10
100
ENERGY (KEV)

FIGURE 7

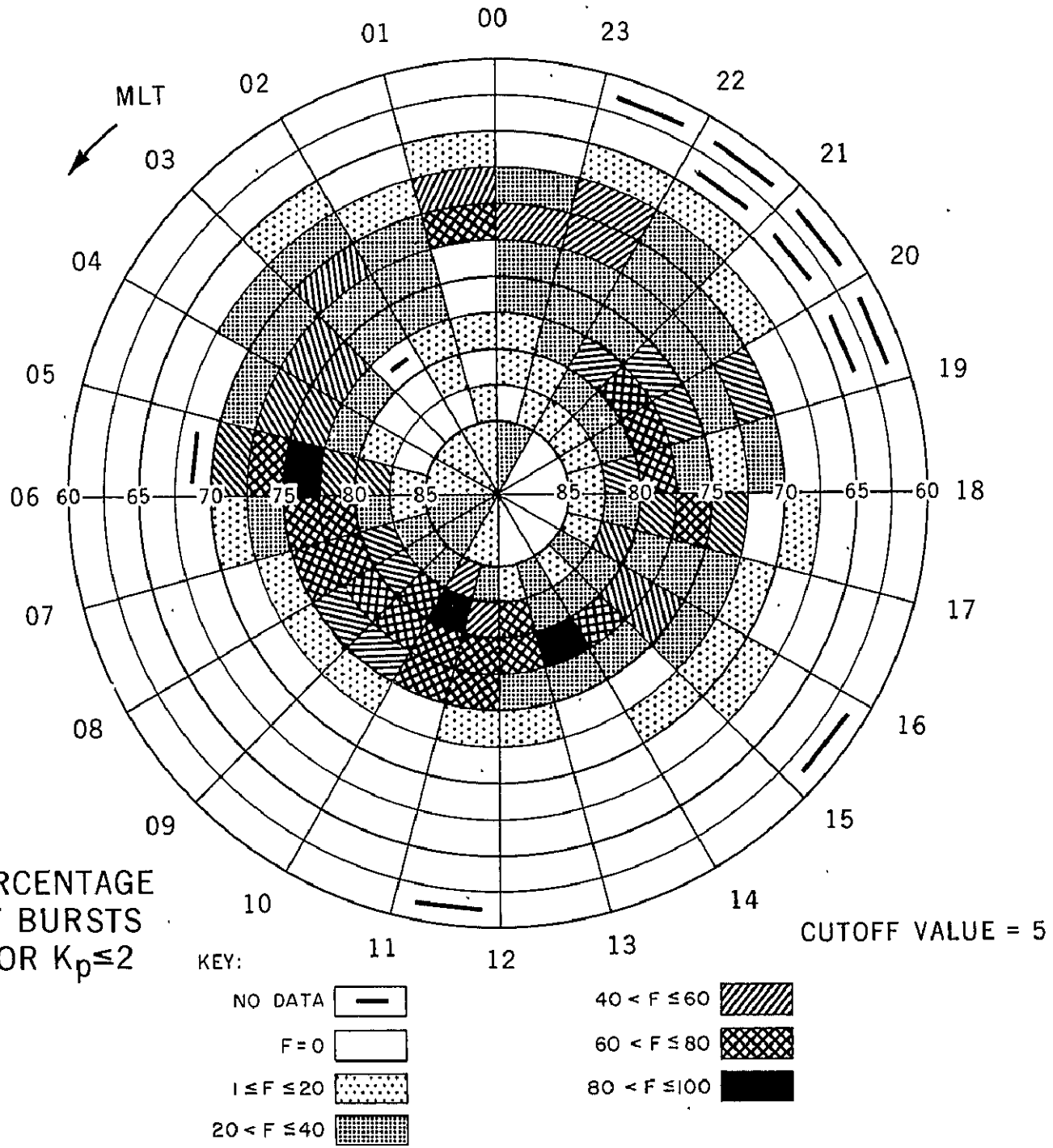
MLT
00
01
02
03
04
05
06
07
08
09
10
11
12
13
14
15
16
17
18
19
20
21
22
23
60
65
70
75
80
85
85
80
75
70
65
60
PERCENTAGE OF BURSTS FOR $K_p \leq 2$
CUTOFF VALUE = 5
KEY:
NO DATA
F = 0
1 ≤ F ≤ 20
20 < F ≤ 40
40 < F ≤ 60
60 < F ≤ 80
80 < F ≤ 100

FIGURE 8

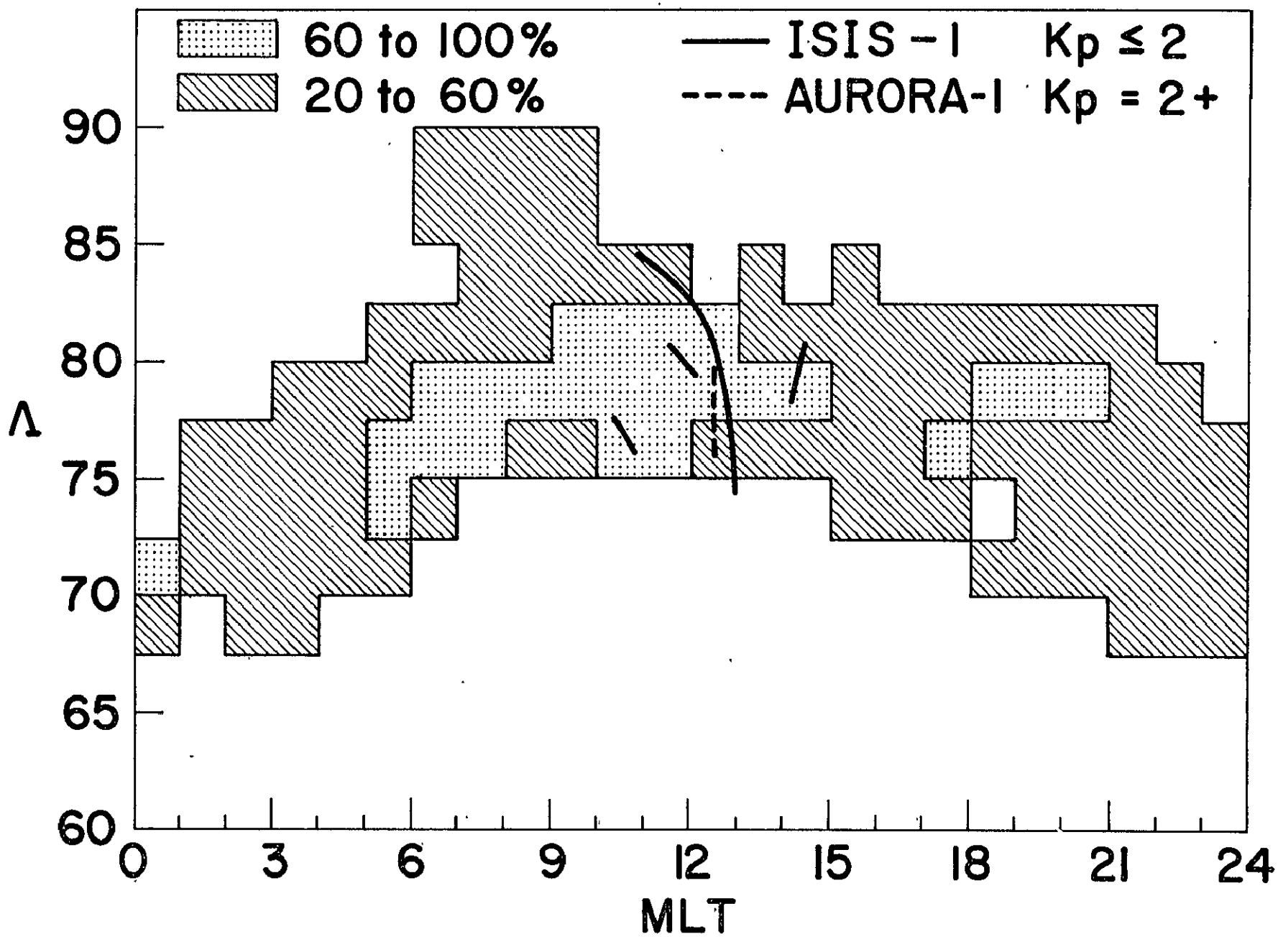
60 to 100%
20 to 60%
ISIS - I Kp ≤ 2
AURORA-I Kp = 2+
90
85
80
75
70
65
60
Λ
0
3
6
9
12
15
18
21
24
MLT

FIGURE 9

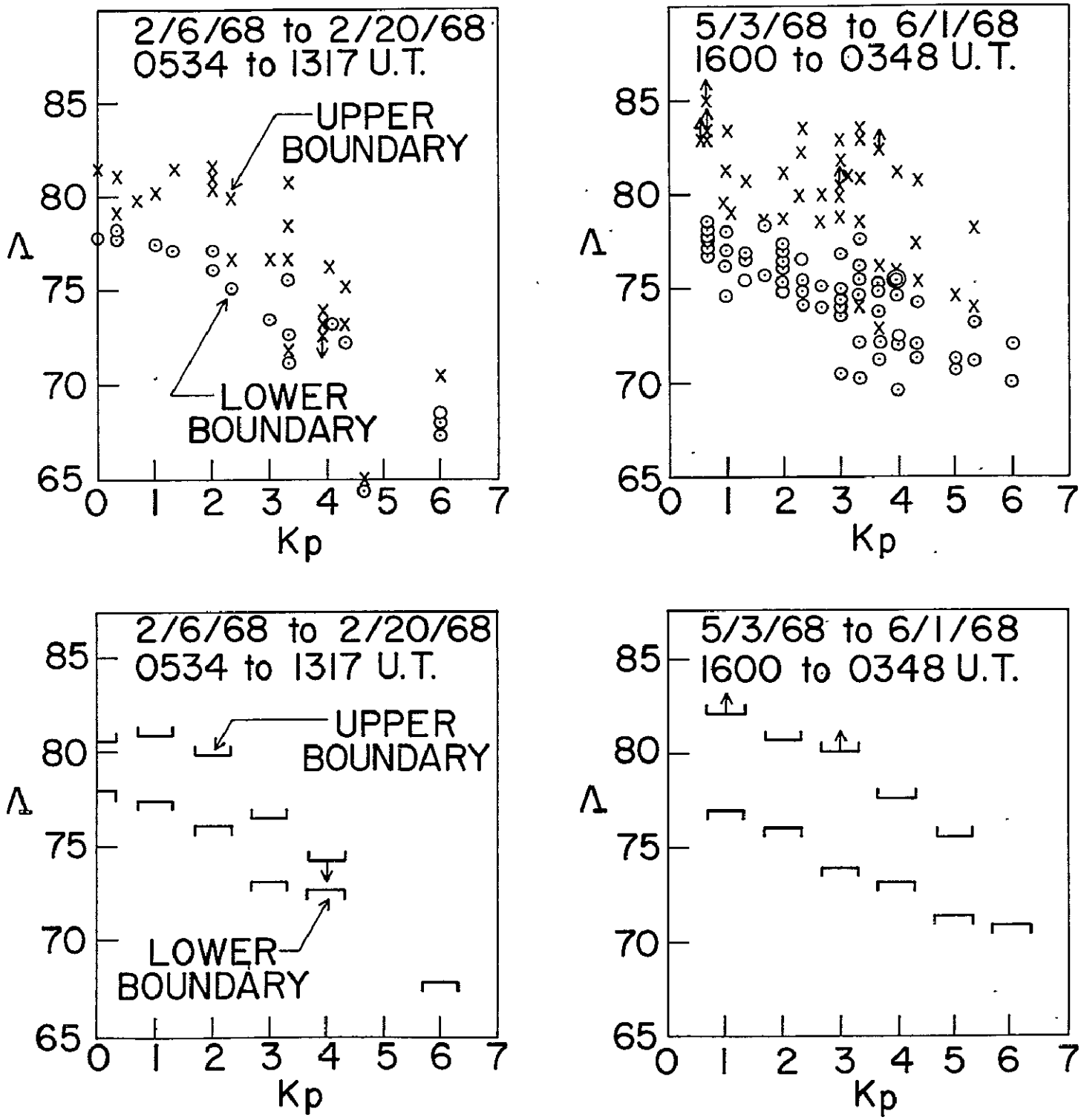
2/6/68 to 2/20/68
0534 to 1317 U.T.
UPPER BOUNDARY
LOWER BOUNDARY
5/3/68 to 6/1/68
1600 to 0348 U.T.
Λ
Kp
85
80
75
70
65
0 1 2 3 4 5 6 7

FIGURE 10

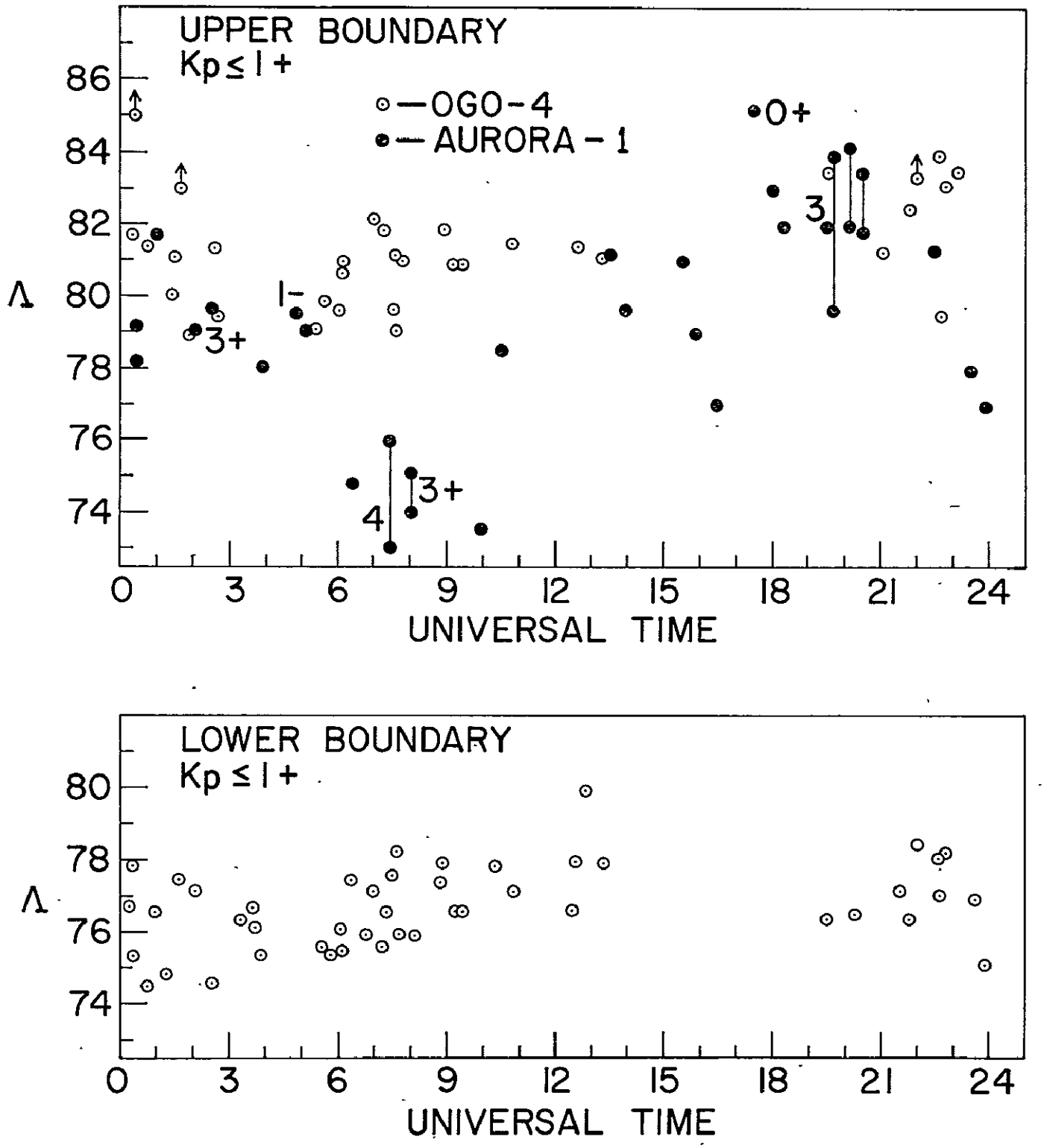
UPPER BOUNDARY
Kp ≤ 1+
⊙—OGO-4
●—AURORA-1
0+
3
1-
3+
4
3+
Λ
86
84
82
80
78
76
74
0
3
6
9
12
15
18
21
24
UNIVERSAL TIME
LOWER BOUNDARY
Kp ≤ 1+
Λ
80
78
76
74
0
3
6
9
12
15
18
21
24
UNIVERSAL TIME

FIGURE 11

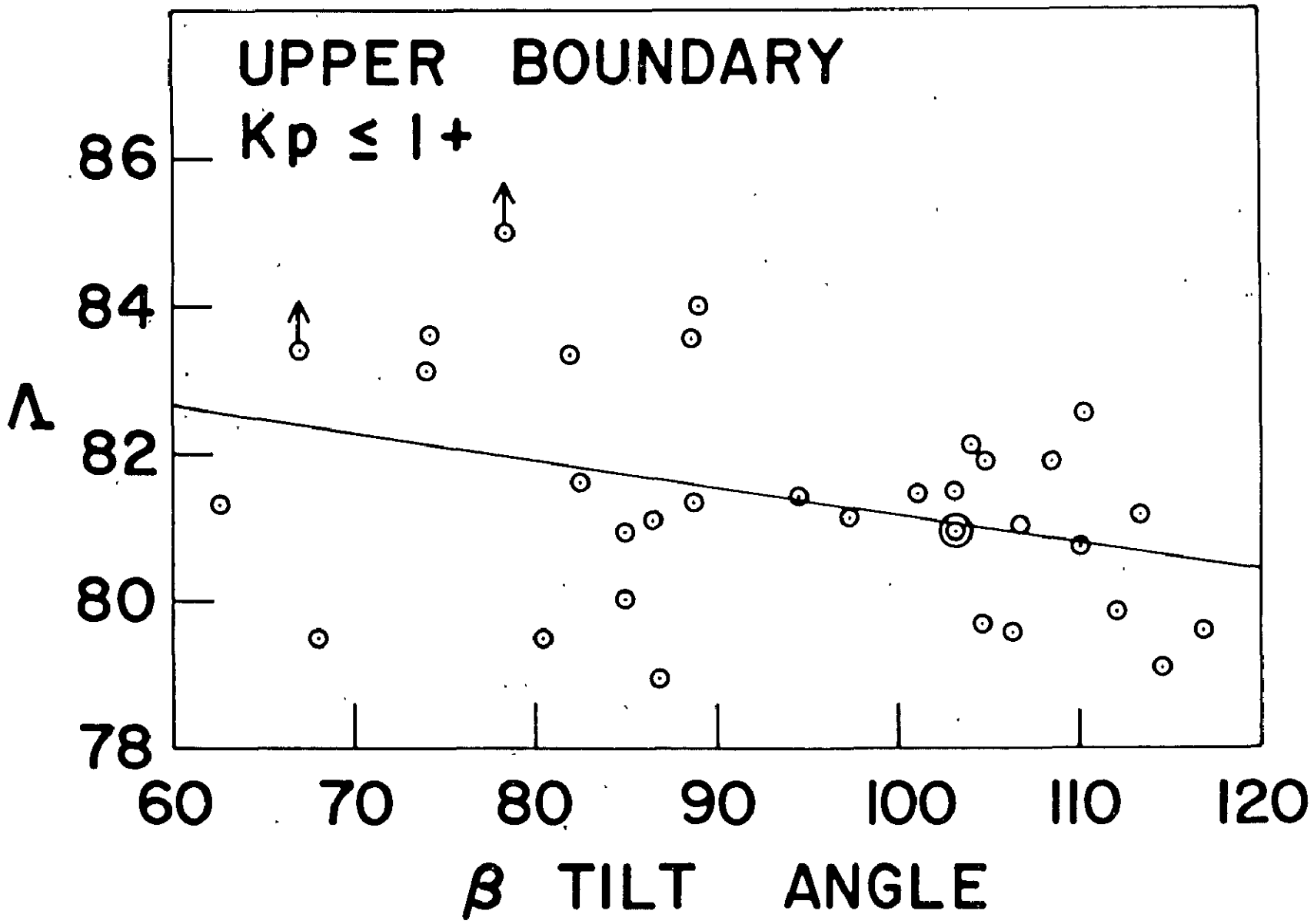
UPPER BOUNDARY
Kp ≤ 1+
86
84
82
80
78
Λ
60
70
80
90
100
110
120
β TILT ANGLE

FIGURE 12

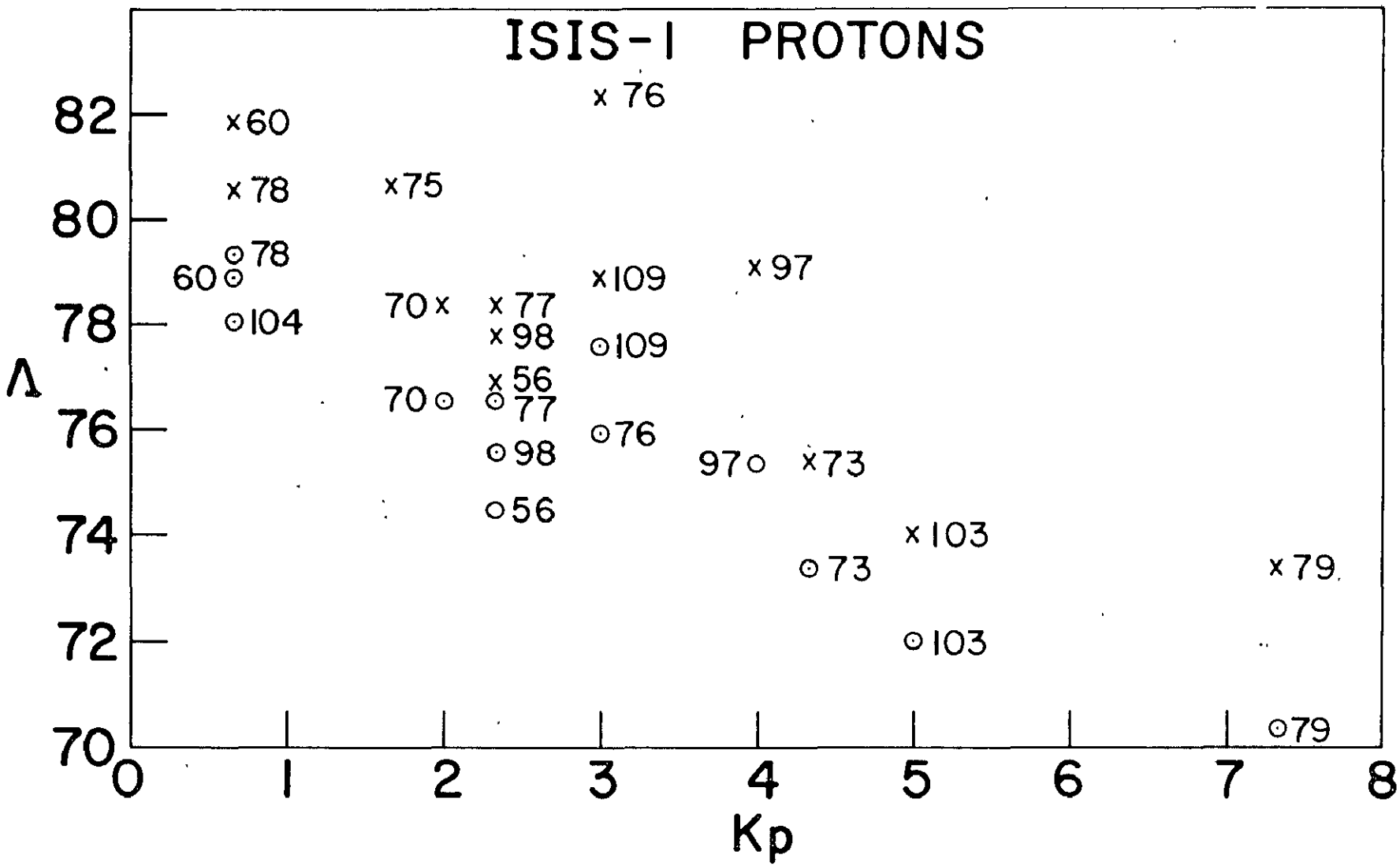
ISIS-1 PROTONS
Λ
Kp
82
80
78
76
74
72
70
0
1
2
3
4
5
6
7
8
x60
x78
x75
x76
x109
x97
x77
x98
x56
x73
x103
x79
⊙78
60⊙
⊙104
70x
70⊙
⊙77
⊙98
⊙56
⊙109
⊙76
97⊙
⊙73
⊙103
⊙79

FIGURE 13

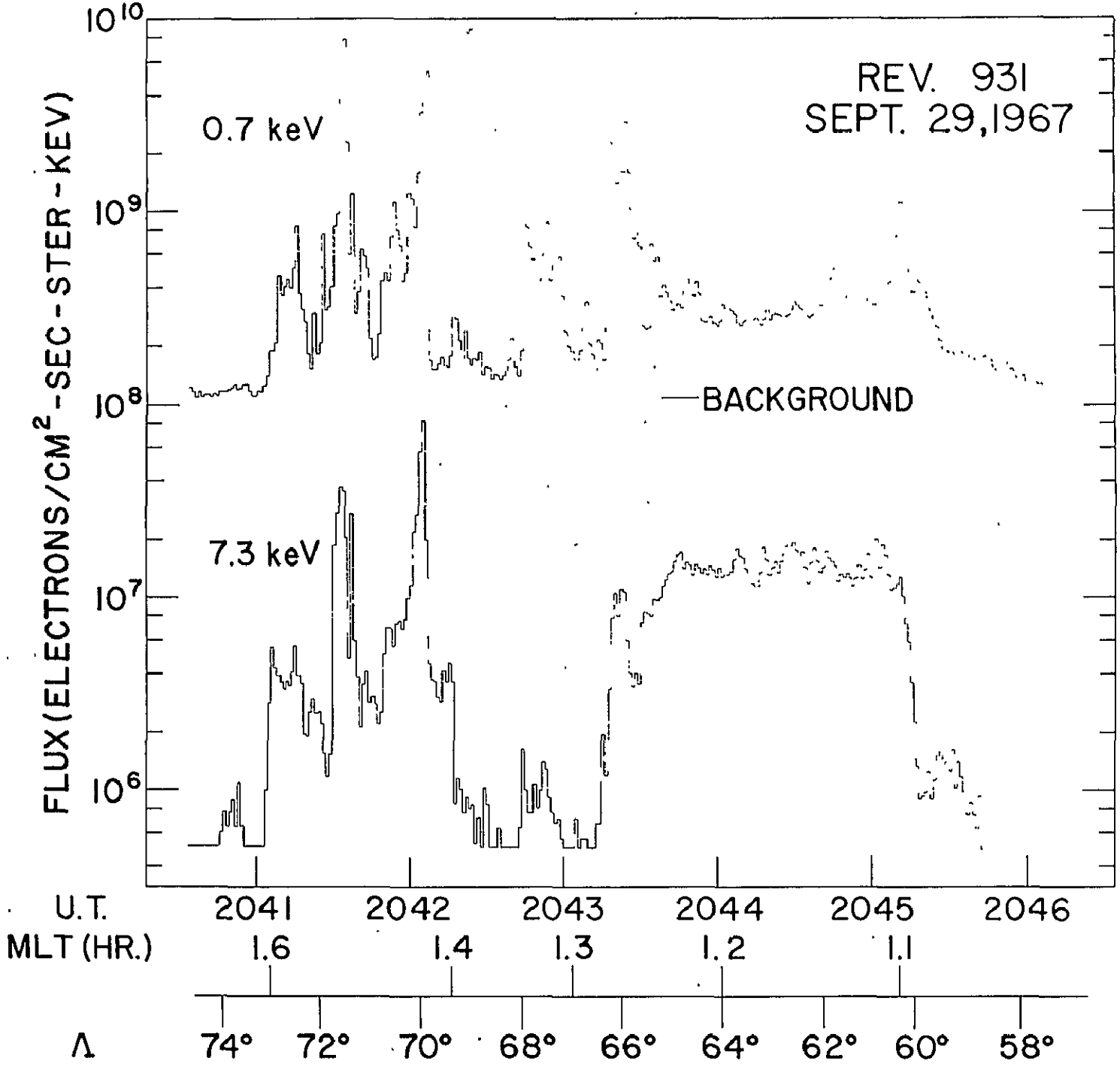
REV. 931
SEPT. 29,1967
0.7 keV
7.3 keV
BACKGROUND
FLUX (ELECTRONS/CM^2-SEC-STER-KEV)
10^{10}
10^9
10^8
10^7
10^6
U.T.
2041
2042
2043
2044
2045
2046
MLT (HR.)
1.6
1.4
1.3
1.2
1.1
Λ
74°
72°
70°
68°
66°
64°
62°
60°
58°

FIGURE 14

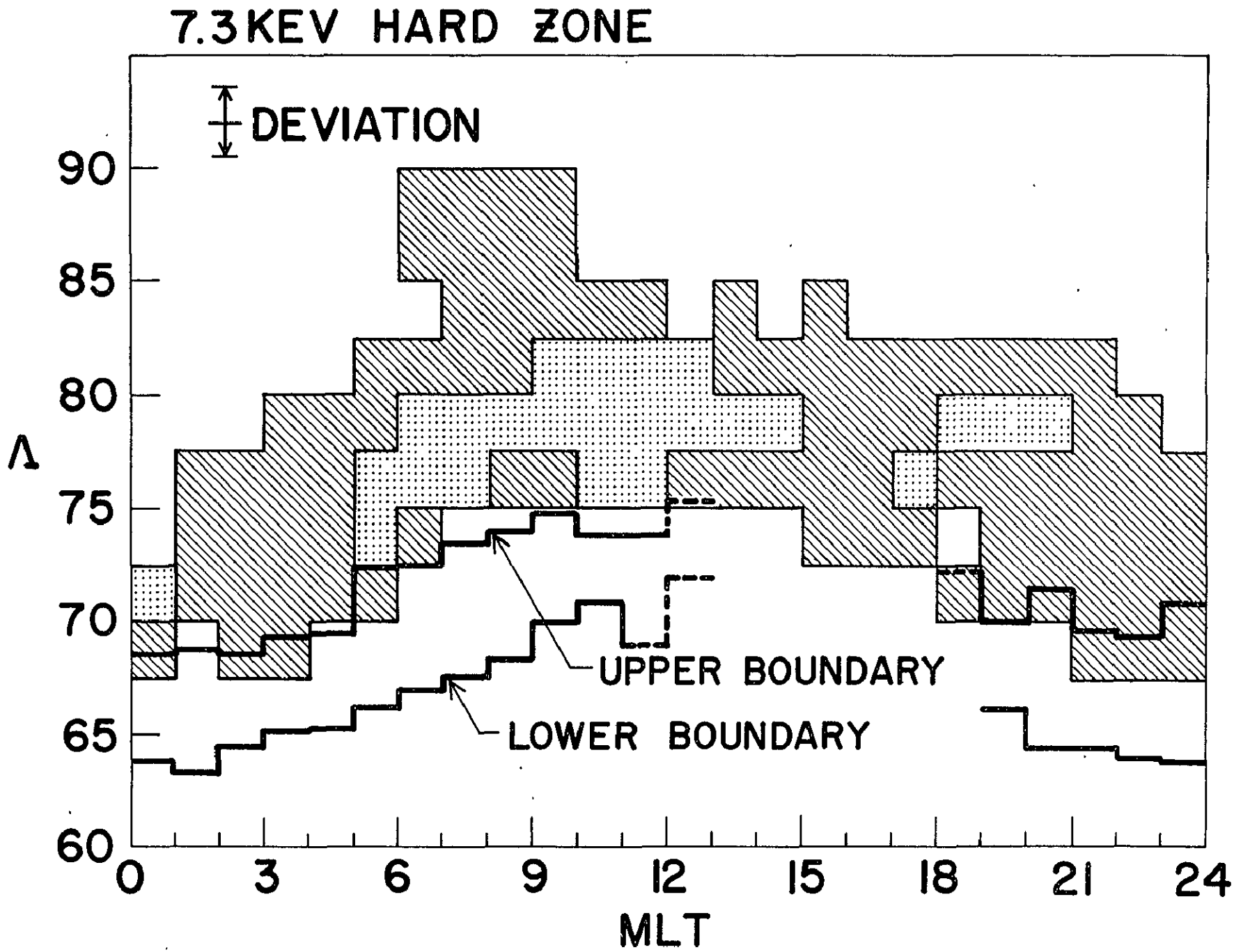
7.3 KEV HARD ZONE
DEVIATION
90
85
80
75
70
65
60
Λ
UPPER BOUNDARY
LOWER BOUNDARY
0
3
6
9
12
15
18
21
24
MLT

FIGURE 15

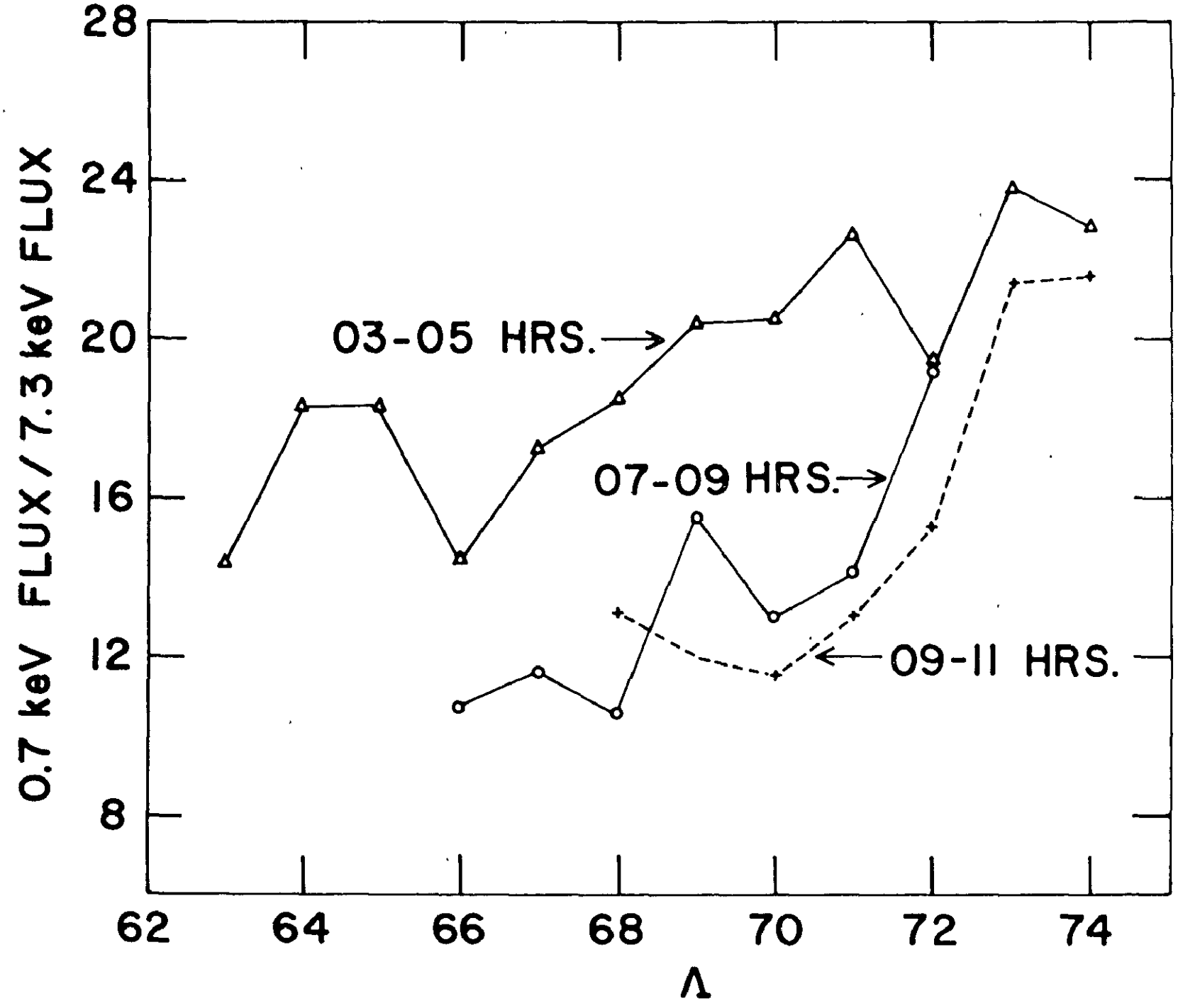
28
24
20
16
12
8
0.7 keV FLUX / 7.3 keV FLUX
03-05 HRS.
07-09 HRS.
09-11 HRS.
62
64
66
68
70
72
74
Λ

FIGURE 16

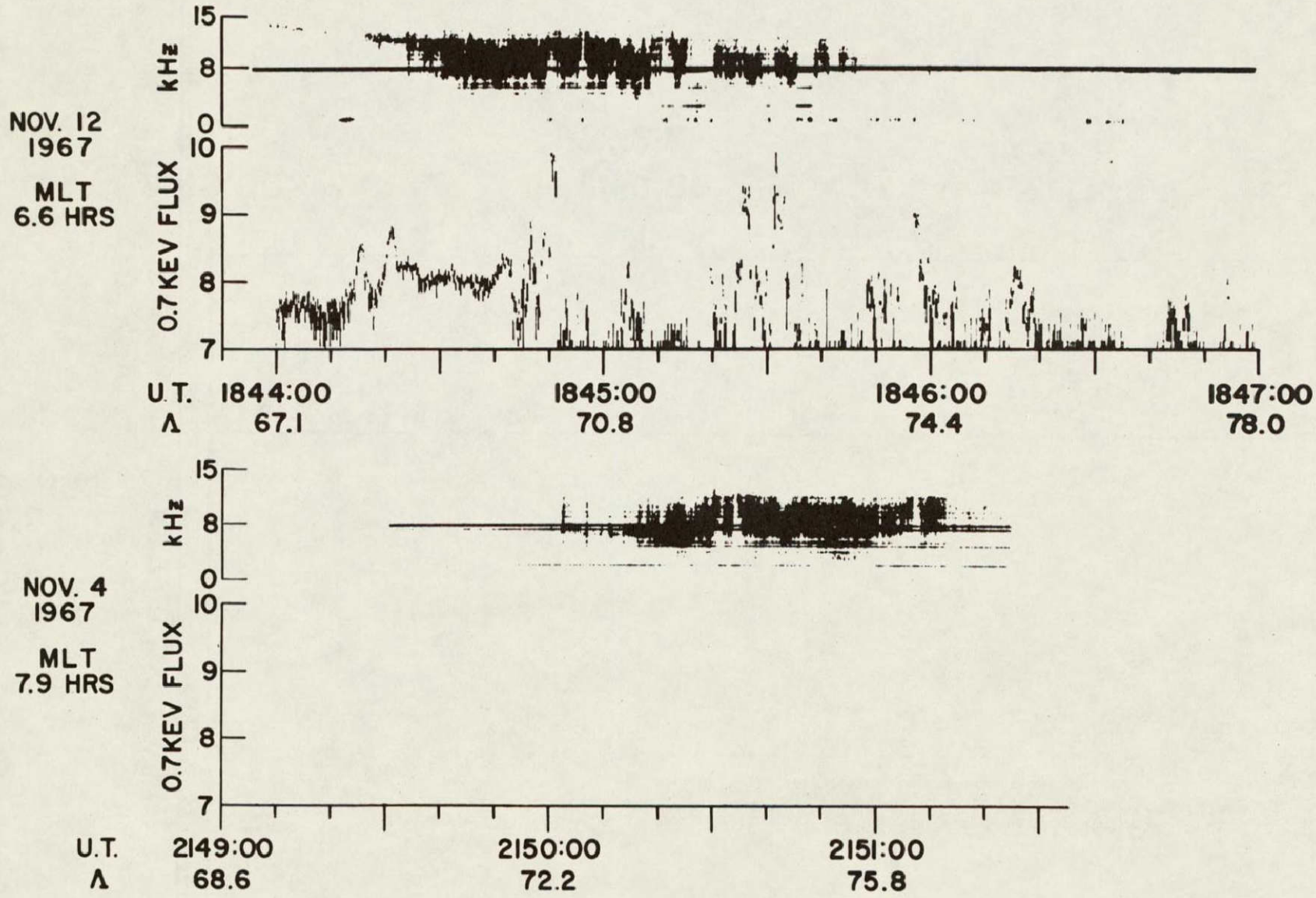
NOV. 12
1967
MLT
6.6 HRS
15
8
0
kHz
10
9
8
7
0.7 KEV FLUX
U.T.
1844:00
1845:00
1846:00
1847:00
Λ
67.1
70.8
74.4
78.0
NOV. 4
1967
MLT
7.9 HRS
15
8
0
kHz
10
9
8
7
0.7KEV FLUX
U.T.
2149:00
2150:00
2151:00
Λ
68.6
72.2
75.8

FIGURE 17

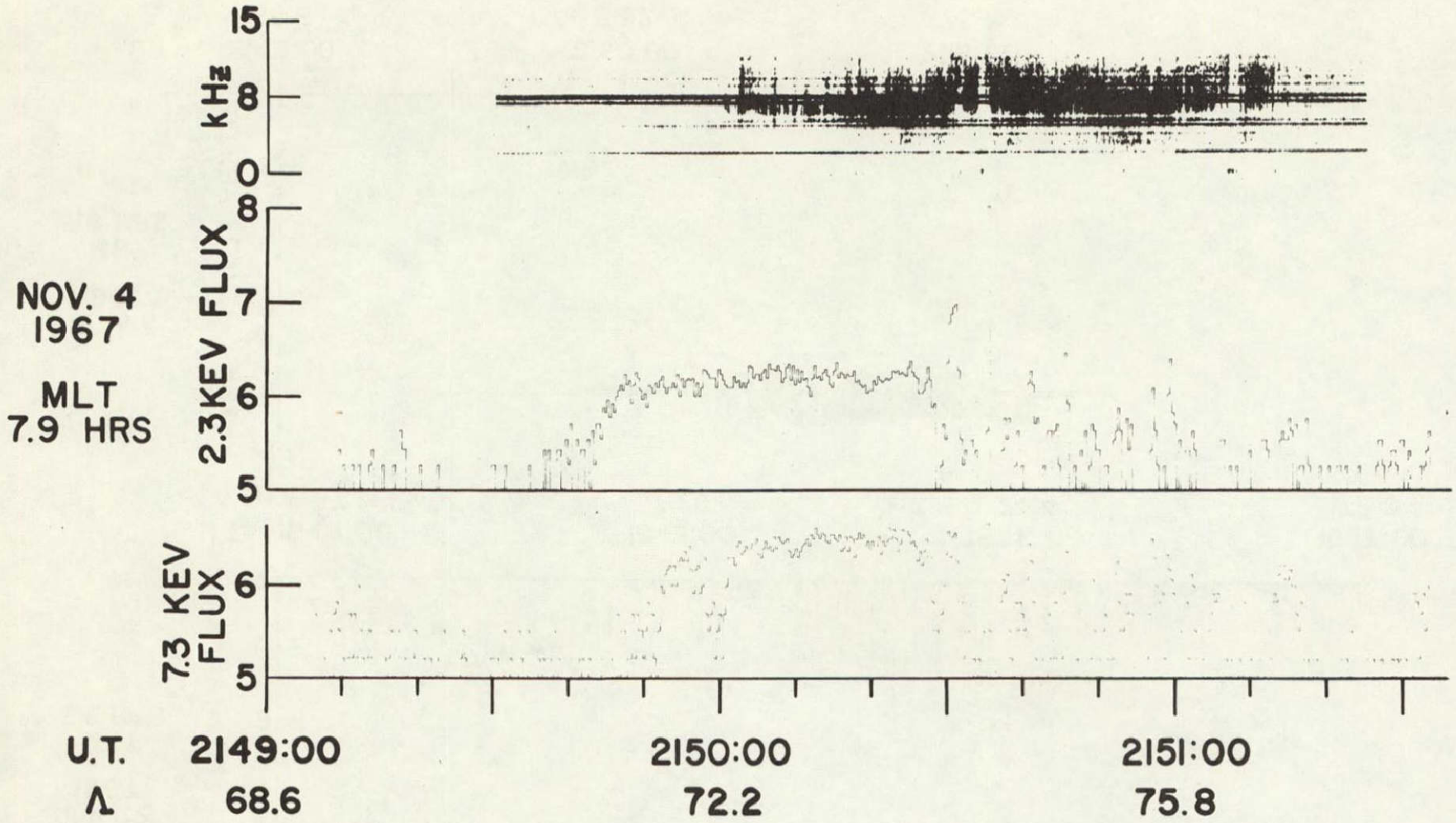
15
8
0
kHz
8
7
6
5
2.3KEV FLUX
NOV. 4
1967
MLT
7.9 HRS
6
5
7.3 KEV
FLUX
U.T.
2149:00
2150:00
2151:00
Λ
68.6
72.2
75.8

FIGURE 18

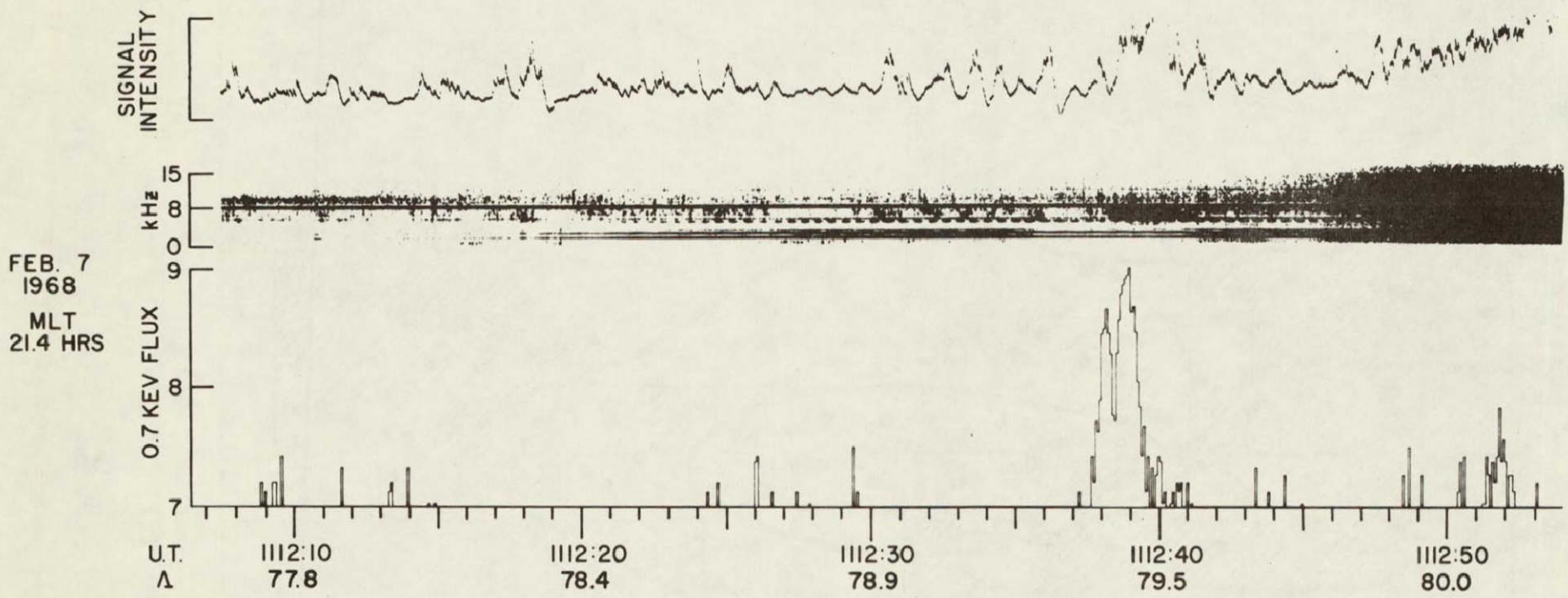
SIGNAL INTENSITY
15
8
0
kHz
FEB. 7
1968
MLT
21.4 HRS
9
8
7
0.7 KEV FLUX
U.T.
Λ
1112:10
77.8
1112:20
78.4
1112:30
78.9
1112:40
79.5
1112:50
80.0

FIGURE 19

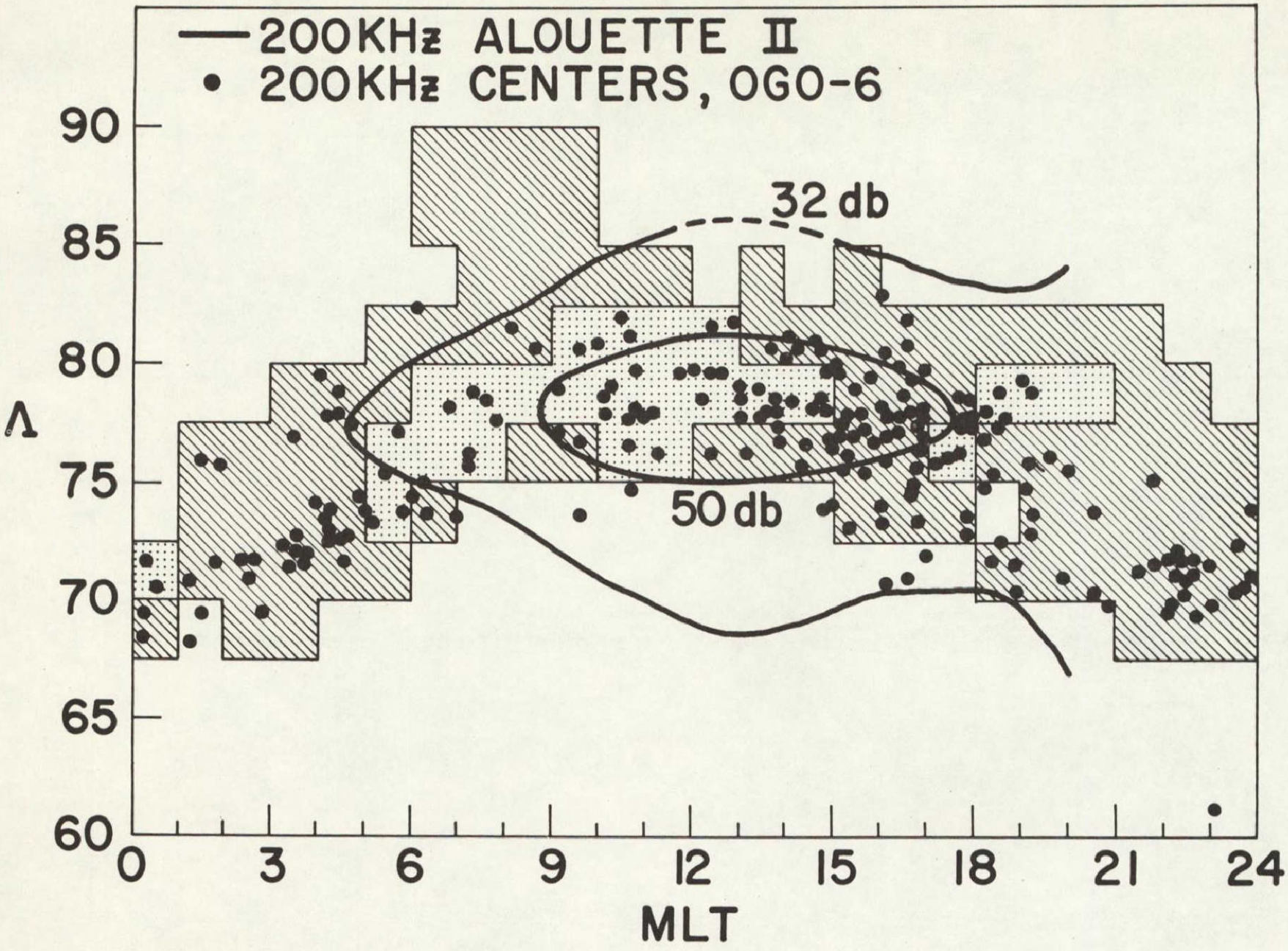
200KHz ALOUETTE II
200KHz CENTERS, OGO-6
32 db
50 db
Λ
90
85
80
75
70
65
60
0
3
6
9
12
15
18
21
24
MLT

FIGURE 20

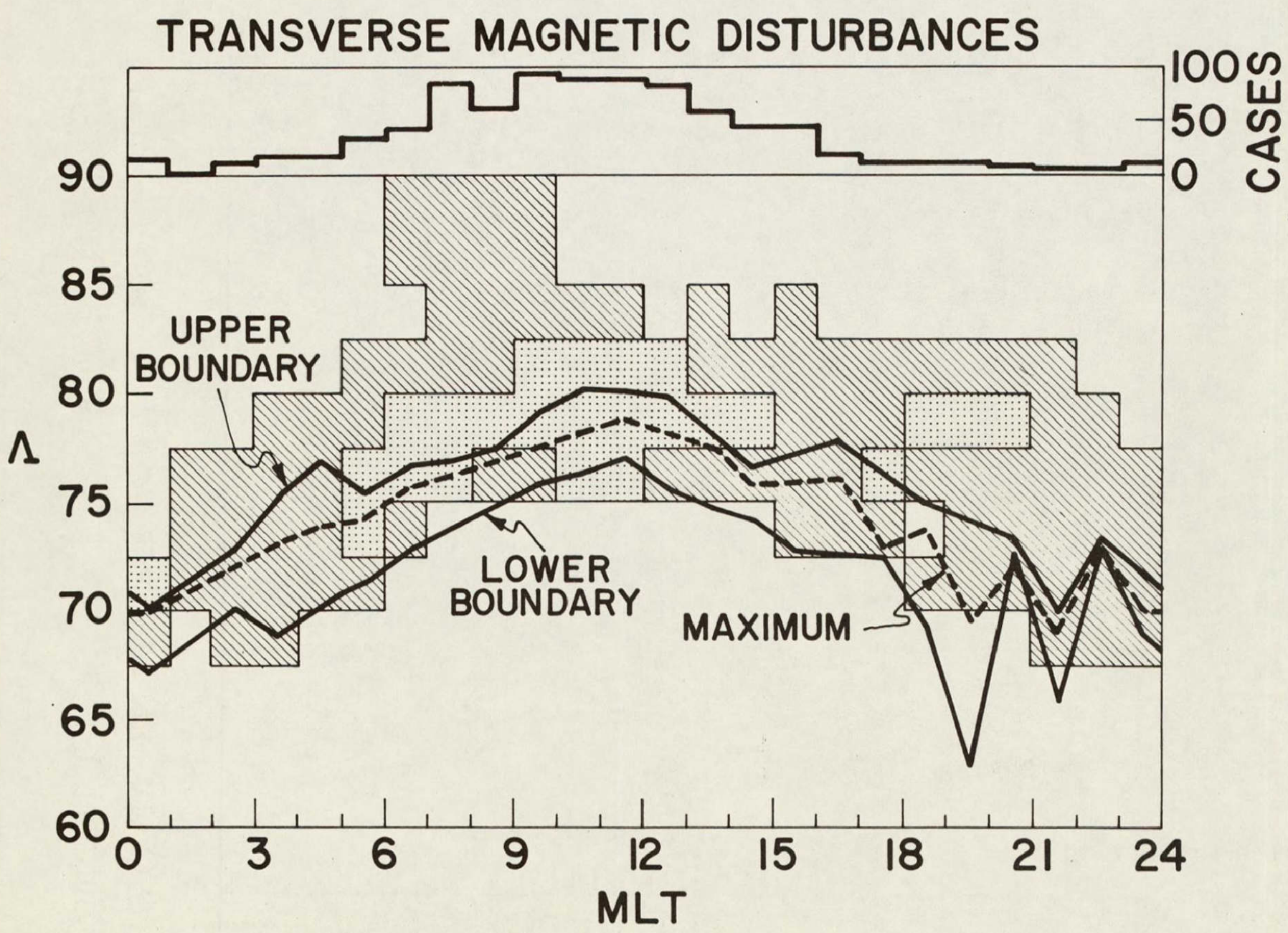
TRANSVERSE MAGNETIC DISTURBANCES
100
50
0
CASES
90
85
80
75
70
65
60
Λ
UPPER
BOUNDARY
LOWER
BOUNDARY
MAXIMUM
0
3
6
9
12
15
18
21
24
MLT

FIGURE 21

FIGURE 22

SEARCH COILS
Z
Y
X
0
5
ELECTRONS
FLUX AT 0.7 KEV
10^{10}
0
2323:45
:50
:55
2324:00
:05

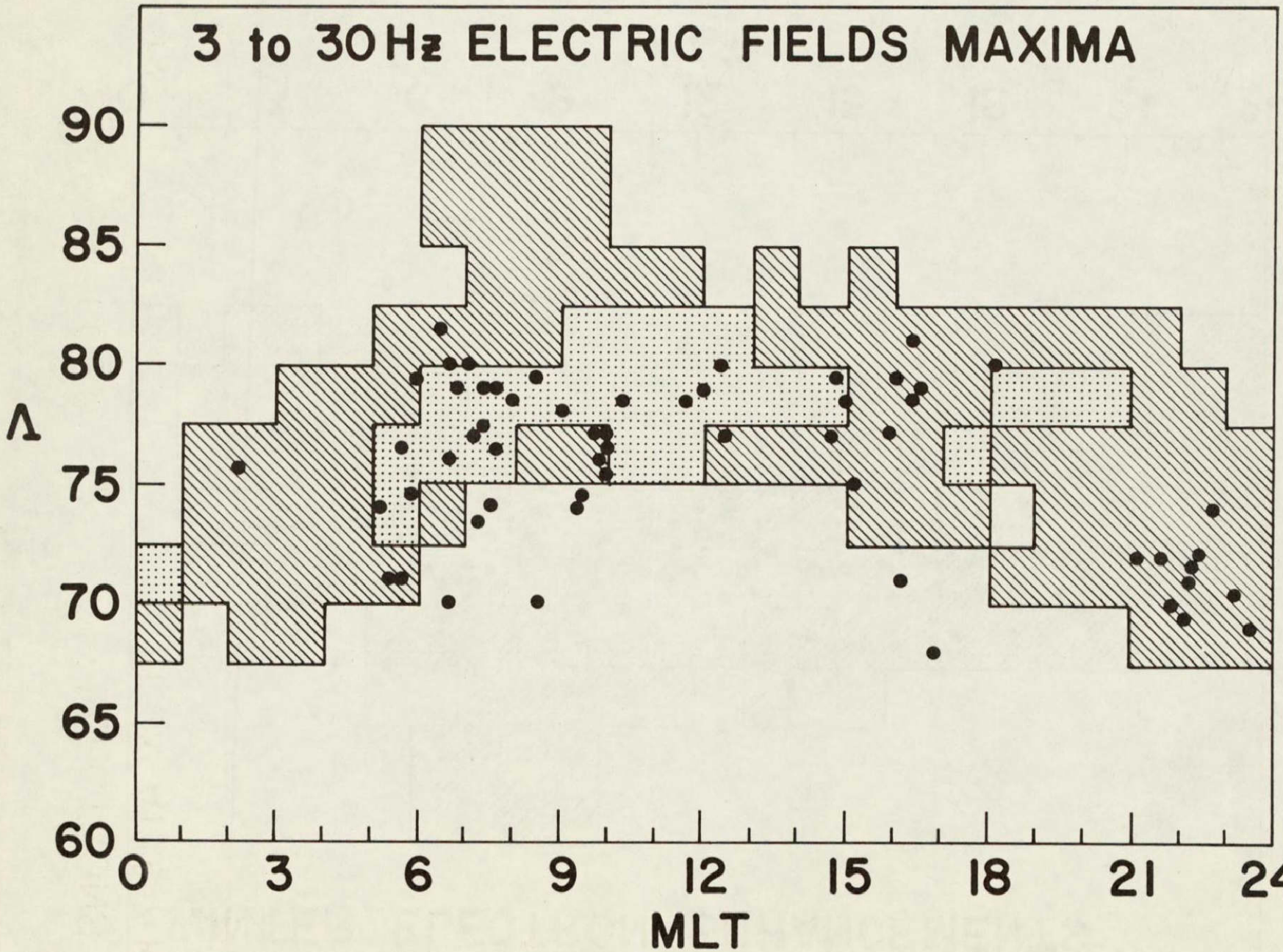
3 to 30 Hz ELECTRIC FIELDS MAXIMA
90
85
80
75
70
65
60
Λ
0
3
6
9
12
15
18
21
24
MLT

FIGURE 23

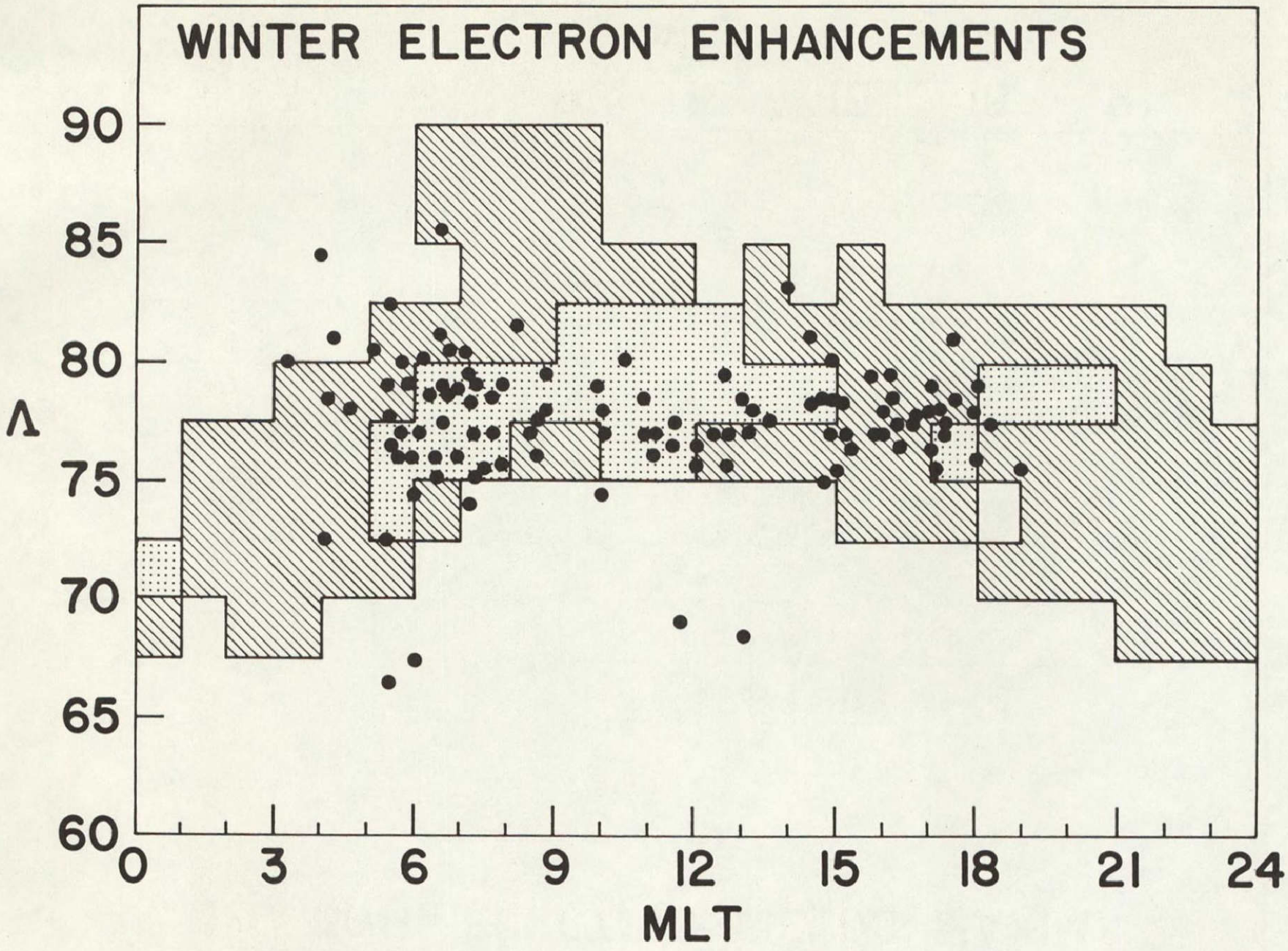
WINTER ELECTRON ENHANCEMENTS
90
85
80
75
70
65
60
Λ
0
3
6
9
12
15
18
21
24
MLT

FIGURE 24

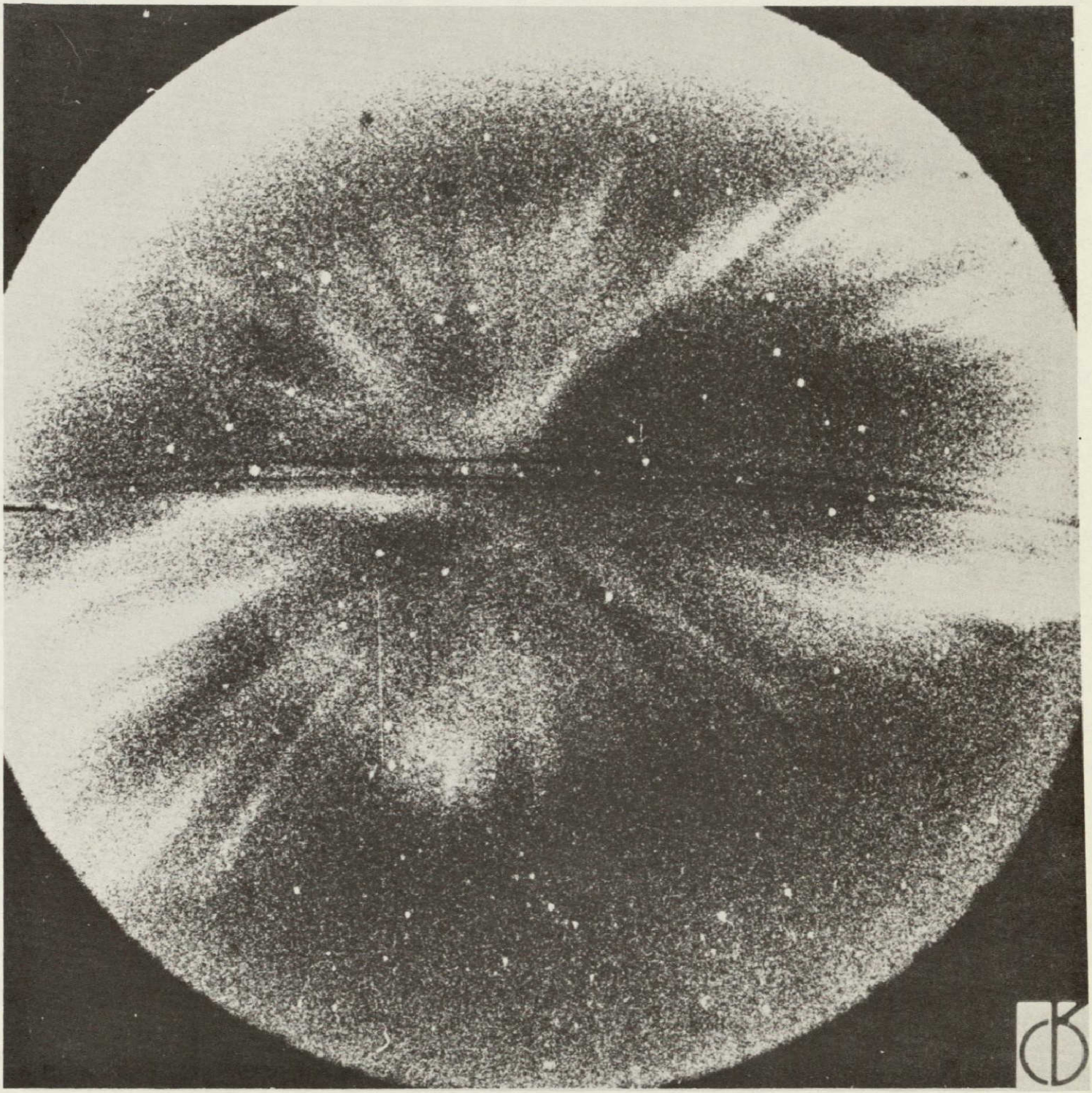

FIGURE 25

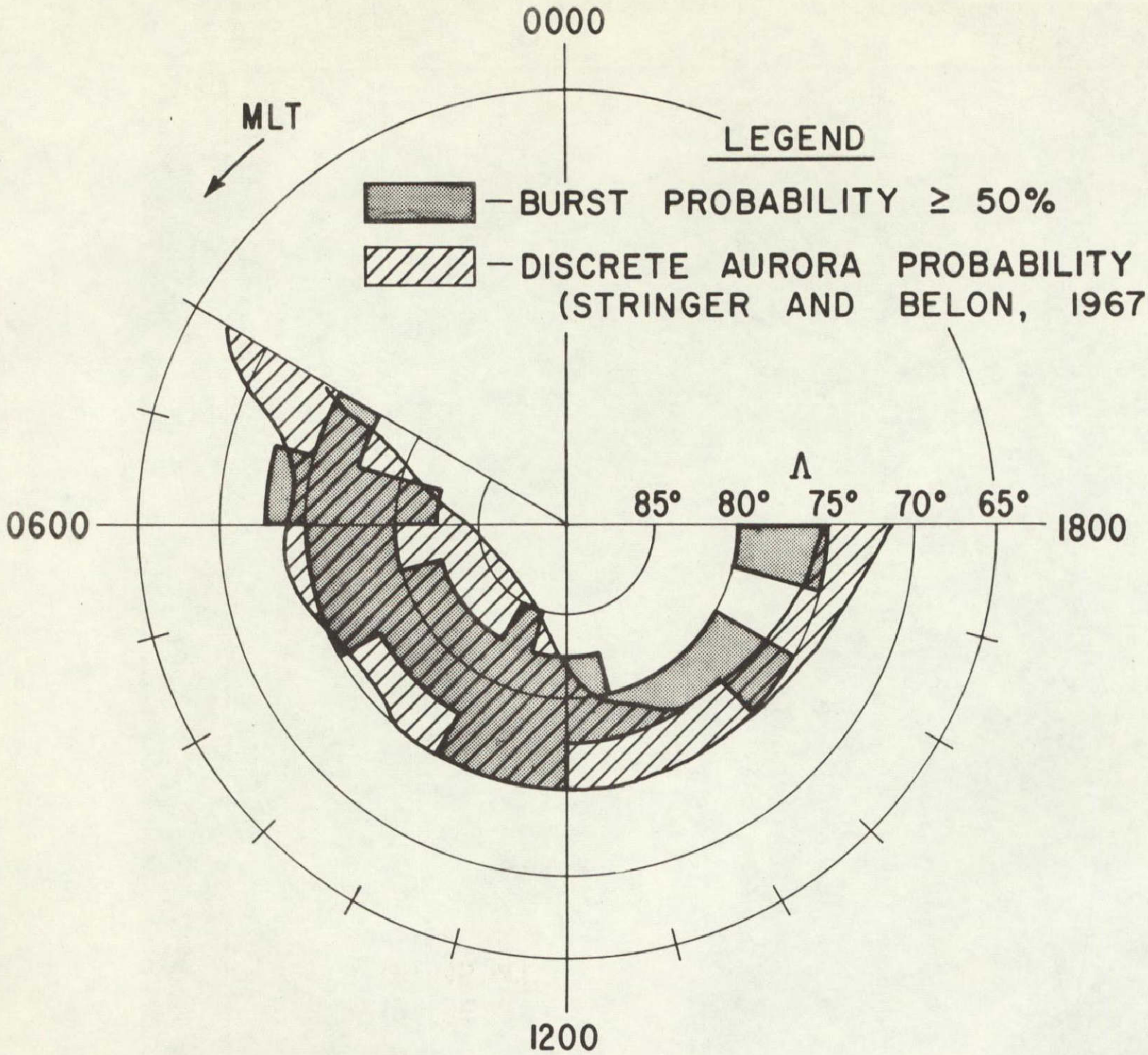
0000
MLT
LEGEND
BURST PROBABILITY ≥ 50%
DISCRETE AURORA PROBABILITY ≥ 15 %
(STRINGER AND BELON, 1967)
Λ
85°
80°
75°
70°
65°
0600
1800
1200

FIGURE 26

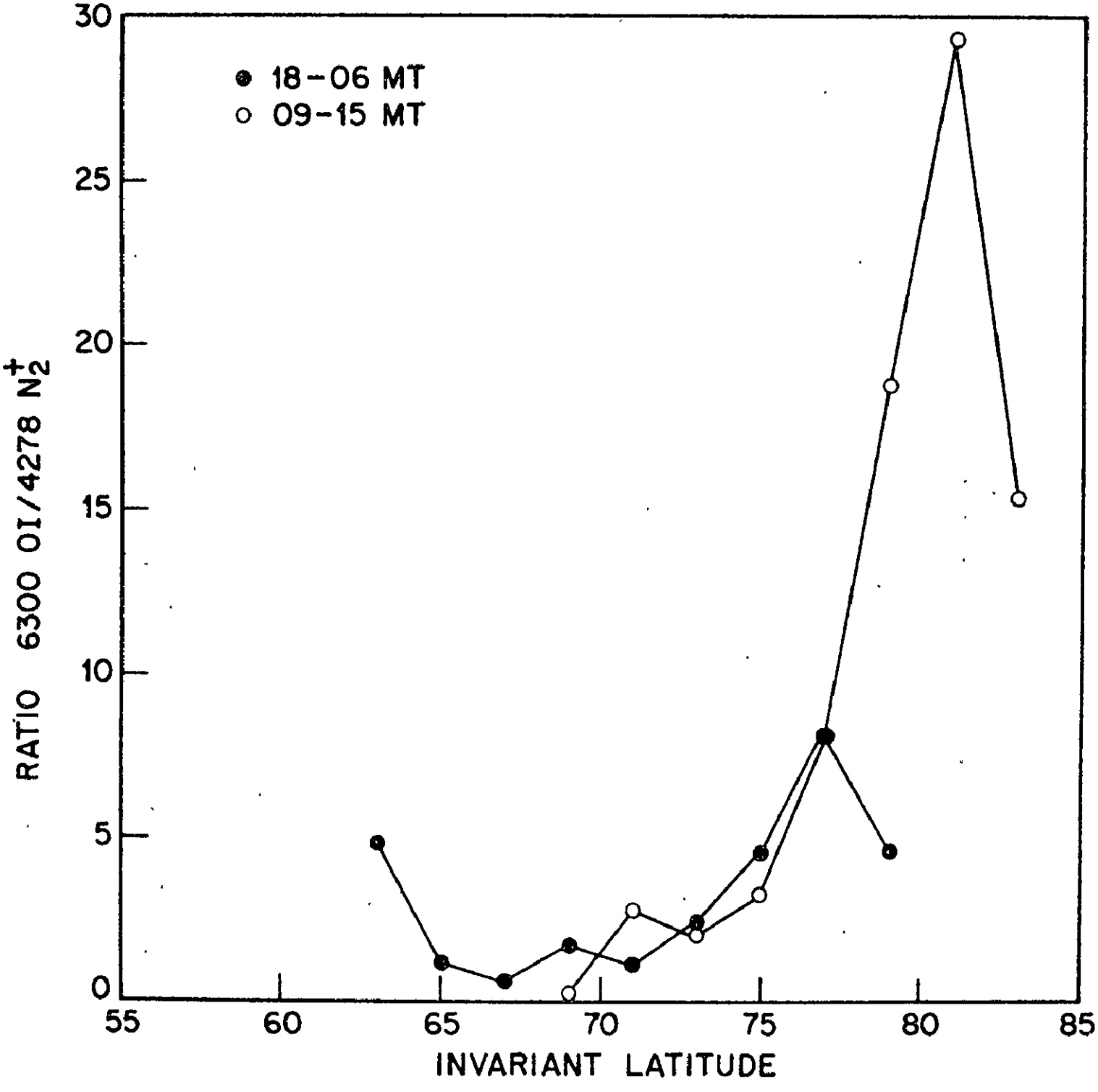
18-06 MT
09-15 MT
RATIO 6300 OI/4278 N_2^+
INVARIANT LATITUDE
0
5
10
15
20
25
30
55
60
65
70
75
80
85

FIGURE 27

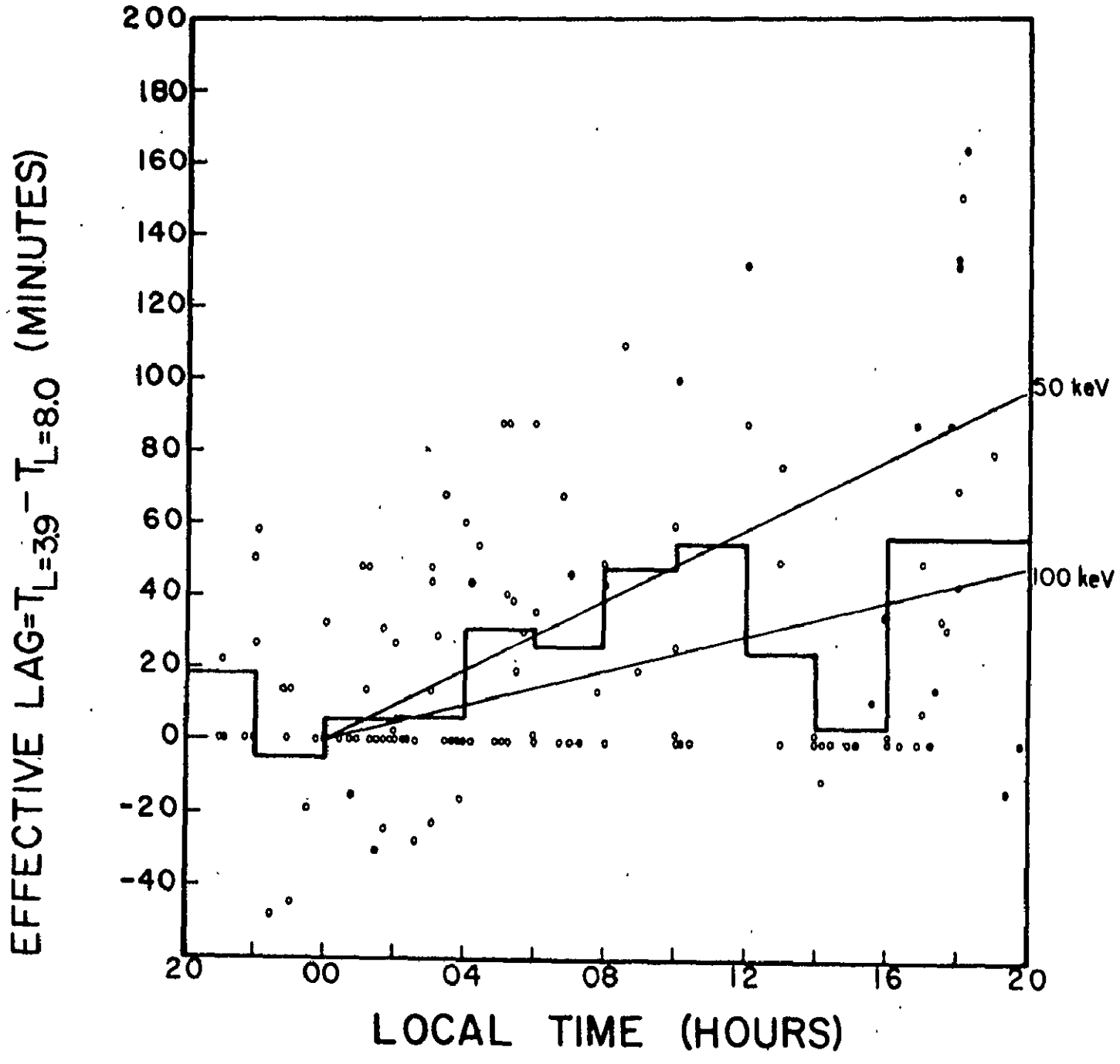
EFFECTIVE LAG=$T_{L=3.9} - T_{L=8.0}$ (MINUTES)
200
180
160
140
120
100
80
60
40
20
0
-20
-40
20
00
04
08
12
16
20
LOCAL TIME (HOURS)
50 keV
100 keV

FIGURE 28

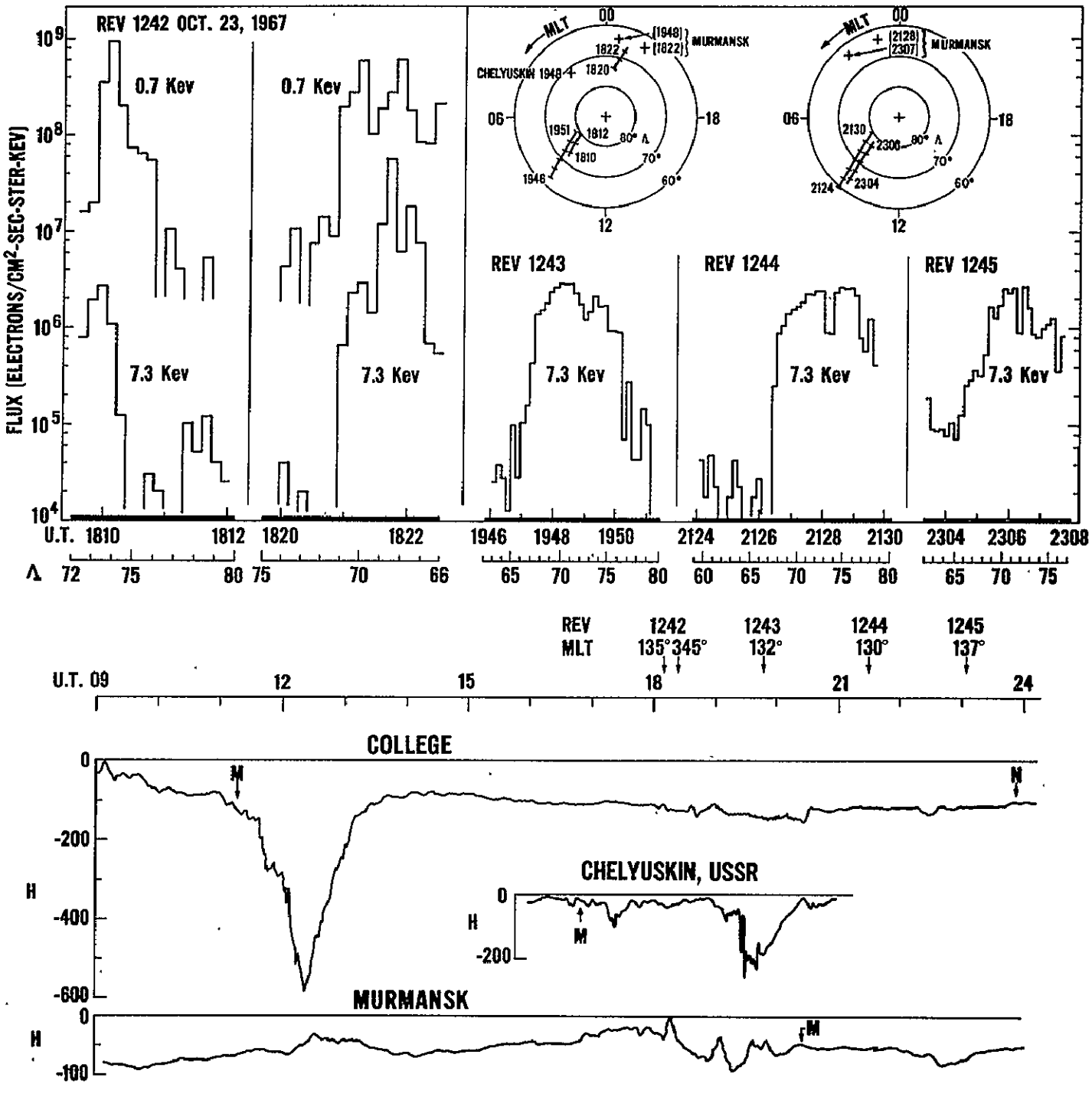
REV 1242 OCT. 23, 1967
FLUX (ELECTRONS/CM²-SEC-STER-KEV)
0.7 Kev
7.3 Kev
0.7 Kev
7.3 Kev
REV 1243
7.3 Kev
REV 1244
7.3 Kev
REV 1245
7.3 Kev
MLT
MURMANSK
CHELYUSKIN
U.T. 1810 1812 1820 1822 1946 1948 1950 2124 2126 2128 2130 2304 2306 2308
Λ 72 75 80 75 70 66 65 70 75 80 60 65 70 75 80 65 70 75
REV 1242 1243 1244 1245
MLT 135° 345° 132° 130° 137°
U.T. 09 12 15 18 21 24
COLLEGE
CHELYUSKIN, USSR
MURMANSK
H

FIGURE 29

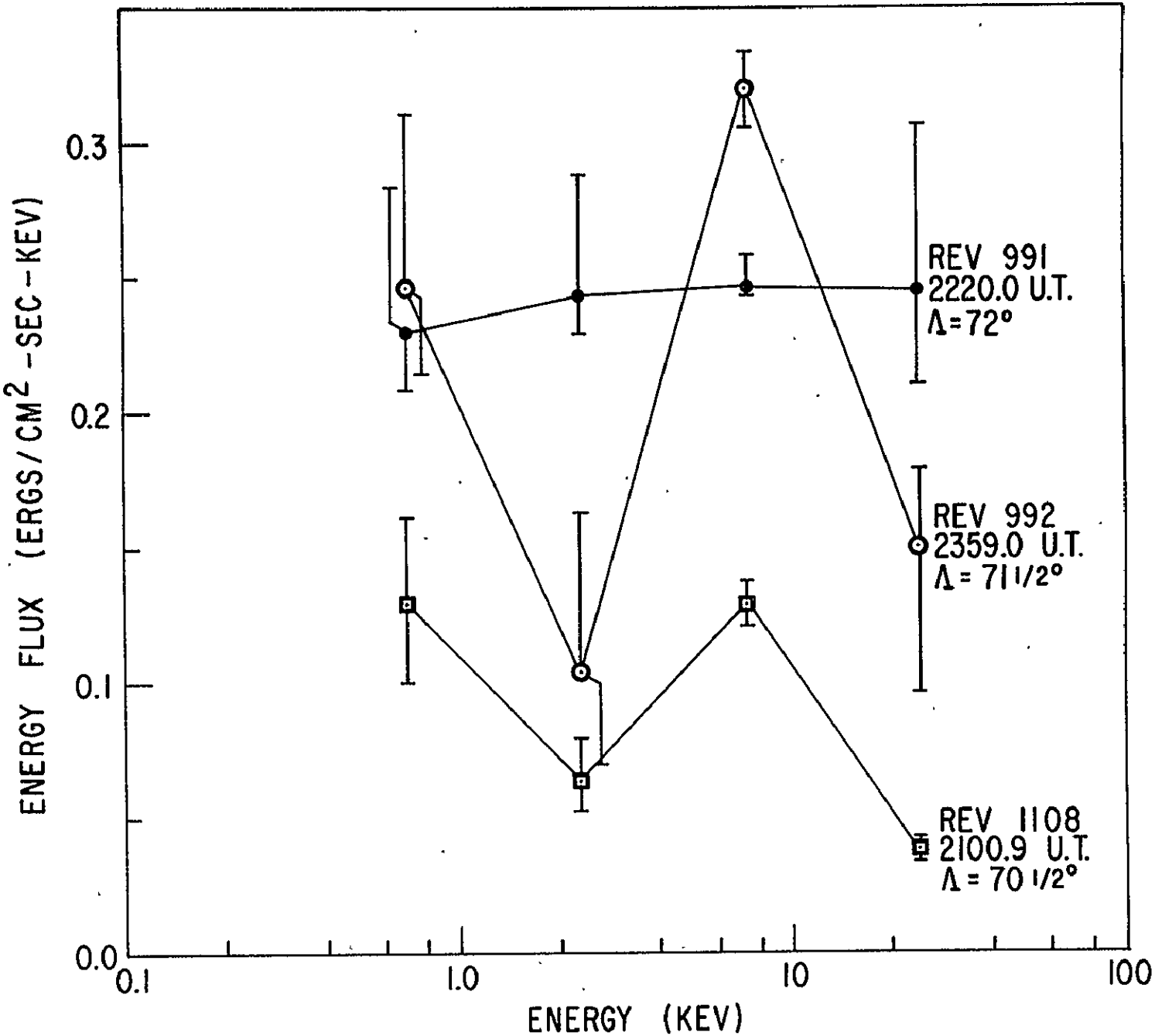
ENERGY FLUX (ERGS/CM^2-SEC-KEV)
0.3
0.2
0.1
0.0
0.1
1.0
10
100
ENERGY (KEV)
REV 991
2220.0 U.T.
Λ=72°
REV 992
2359.0 U.T.
Λ = 71 1/2°
REV 1108
2100.9 U.T.
Λ = 70 1/2°

FIGURE 30

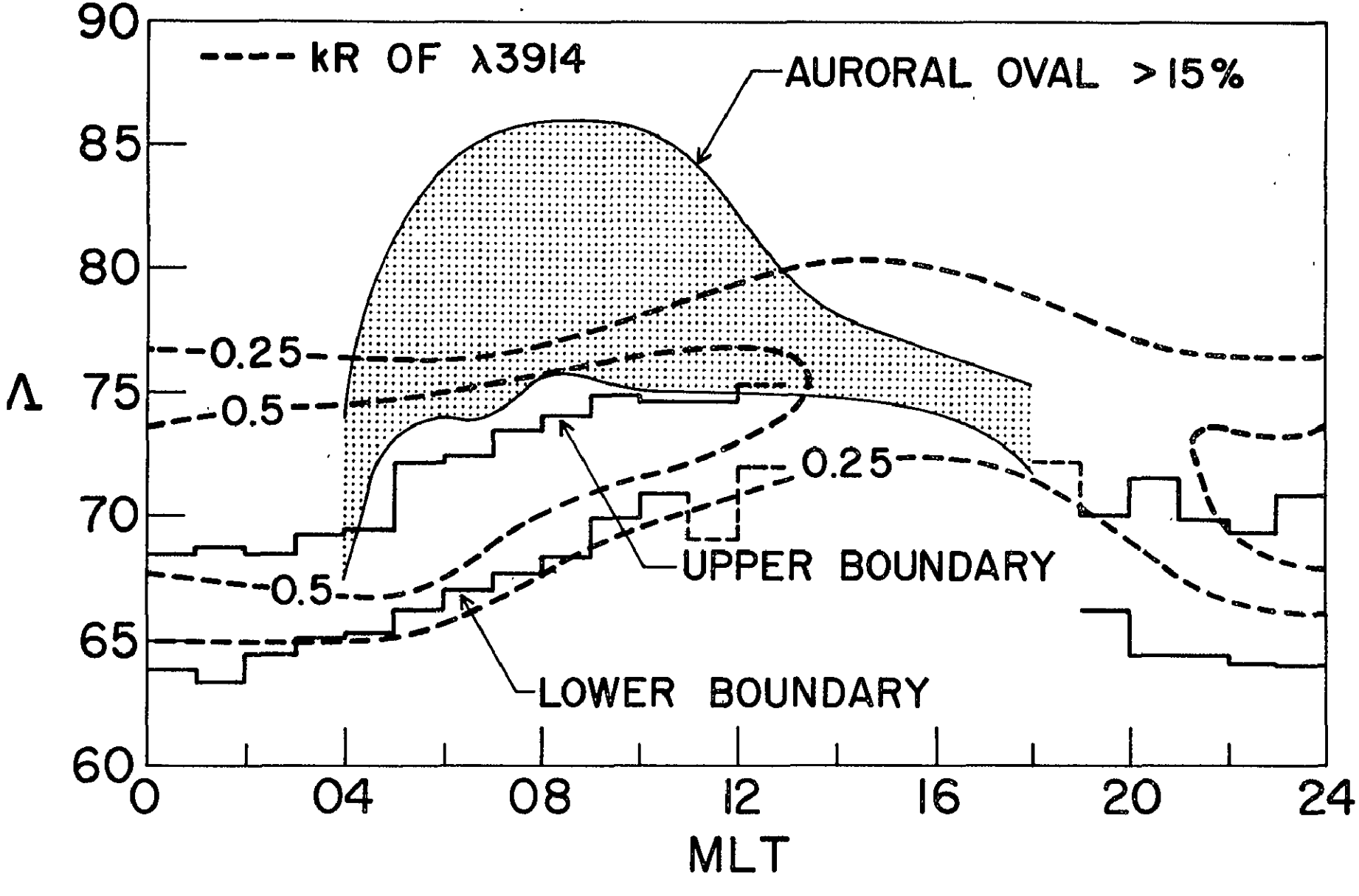
90
85
80
75
70
65
60
Λ
---- kR OF λ3914
AURORAL OVAL >15%
0.25
0.5
0.5
0.25
UPPER BOUNDARY
LOWER BOUNDARY
0
04
08
12
16
20
24
MLT

FIGURE 31